

Masked Modulation: High-Throughput Half-Duplex ISAC Transmission Waveform Design

Yifeng Xiong, *Member, IEEE*, Junsheng Mu, *Member, IEEE*, Shuangyang Li, *Member, IEEE*, Marco Lops, *Fellow, IEEE*, and Jianhua Zhang, *Senior Member, IEEE*

Abstract—Integrated sensing and communication (ISAC) enables numerous innovative wireless applications. Communication-centric design is a practical choice for the construction of the sixth generation (6G) ISAC networks. Continuous-wave-based ISAC systems, with orthogonal frequency-division multiplexing (OFDM) being a representative example, suffer from the self-interference (SI) problem, and hence are less suitable for long-range sensing. On the other hand, pulse-based half-duplex ISAC systems are free of SI, but are also less favourable for high-throughput communication scenarios.

In this treatise, we propose MASKed Modulation (MASM), a half-duplex ISAC waveform design scheme, which minimises a range blindness metric, referred to as “range glint”, given a duty cycle (proportional to communication throughput) constraint. In particular, MASM is capable of supporting high-throughput communication ($\sim 50\%$ duty cycle) under mild range glint. Moreover, MASM can be flexibly adapted to frame-level waveform designs by operating on the slow-time scale. In terms of optimal transmit mask design, a set of masks is shown to be *ideal* in the sense of sidelobe level and range glint intensity.

Index Terms—Integrated sensing and communication, blind range mitigation, half duplex, long-range sensing.

I. INTRODUCTION

INTEGRATED sensing and communication (ISAC) has been envisioned by the International Telecommunication Union as one of the six major usage scenarios in the sixth generation (6G) wireless networks [1]. By coordinating wireless resources such as waveform, hardware platform, time, bandwidth, beam, and energy in a unified manner, ISAC provides an elegant and resource-efficient solution to emerging applications requiring both sensing and communication services, including autonomous driving, low-altitude economy, and human activity sensing [2]–[5].

Among all ISAC design paradigms, the communication-centric strategy is arguably the most favourable approach to 6G ISAC networks, which aims for implementing sensing functionalities by imposing minimal modifications on existing communication infrastructures and protocols. Since the publication of the seminal contribution [6], a large body of literature has been devoted to the design of communication-centric schemes [7]–[11]. Due to the convenience of implementation, early endeavours on this direction performed sensing relying on pilot symbols for channel estimation [12]. To fully unleash the sensing potential of communication signals, recent works further took data payload signals into account [11], [13]–[15]. Notably, the authors of [11] have shown that OFDM is the optimal communication-centric ISAC waveform for data payload signals, in the sense that it achieves the lowest ranging sidelobe.

Despite their convenience, communication-centric ISAC waveforms in their original form may not exhibit satisfactory long-range sensing capability, which is crucial for

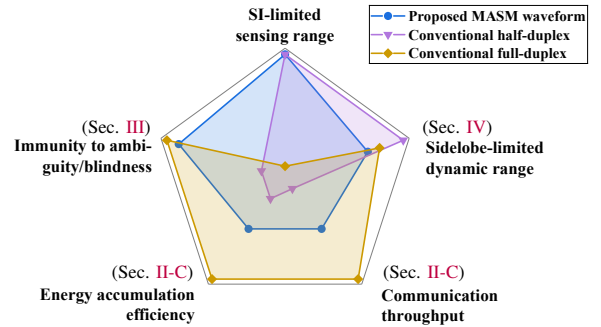


Fig. 1. Qualitative performance comparison between proposed MASM waveforms and conventional ISAC waveforms.

applications such as surveillance of low-altitude unmanned aerial vehicles (UAVs). To elaborate, due to the insufficient transmitter-receiver isolation, straightforward utilisation of the communication-oriented signals for sensing would suffer from self-interference (SI), thereby exhibiting limited sensing range. In its essence, the SI issue originates from the fact that the sensing subsystem operates in a *full-duplex* mode, which receives echoes while transmitting communication signals. Such problems have been discussed extensively in the communication literature [16]–[19] but remain far from being completely resolved.

In the radar literature, a classical solution to SI is to use pulse radars, which switch off the receiver upon transmission. Such transmission schemes are often referred to as *half-duplex* schemes in the communication literature [20]. Since echoes returned during transmission cannot be received, the pulses employed in pulse radars are typically narrow to ensure relatively small blind ranges. Consequently, pulse radars designed for ranging typically have small duty cycles ($\leq 10\%$) [21, Chap. 19]. Nevertheless, in the context of ISAC, the requirement of high-throughput communication motivates large duty cycle designs that can carry more data symbols on the pulses.

To tackle this sensing-communication tradeoff, a possible approach is to first increase the duty cycle (resulting in higher pulse repetition frequency (PRF)), and then mitigate the range ambiguity issue using PRF staggering [22]–[25]. The main idea of PRF staggering methods is to jointly use a set of different PRFs, favourably being co-prime with one another. Since the length of consecutive pulse repetition intervals (PRIs) are different, target echoes delayed longer than a single PRI can be resolved. Besides long-range ranging, PRF staggering techniques are also applied to mitigate the Doppler ambiguity issue (also known as “blind speed”) in moving target indicator (MTI) radars [22]. The main drawback of PRF staggering methods is that there is a lack of principled design methods

of the stagger ratios, namely the ratio between the PRIs. Furthermore, they typically introduce deleterious fluctuations (“ripples” [25]) to the target response spectrum. In light of this, a systematic waveform design approach striking favourable sensing-communication tradeoffs is highly desirable.

Against the aforementioned background, in this treatise, we propose a half-duplex ISAC waveform design scheme, termed as MASKed Modulation (MASM). In particular, MASM designs transmission masks minimizing a range blindness metric, referred to as “range glint”, given a communication throughput (or equivalently, duty cycle) constraint. In each PRI, the system transmits when the mask entry equals to 1, and receives when it equals to 0. It is worth highlighting that the proposed design is capable of supporting relatively high-throughput communication ($\sim 50\%$ duty cycle) under small blind ranges and mild range ambiguity. A qualitative illustration of the performance of MASM waveforms can be seen in Fig. 1, with conventional half-duplex (i.e., pulse radar) and full-duplex schemes being benchmarks.

The main contributions of this treatise are:

- We characterise the range glint effect by defining the metrics of range glint intensity (RGI) and averaged range glint intensity (ARGI), and highlight that it is a unique phenomenon concerning half-duplex sensing schemes;
- We derive explicit closed-form expressions for the expected ARGI of conventional pulse radars and MASM, and formulate the range glint mitigation problem as an ℓ_4 -norm minimisation problem;
- We prove that under certain configurations of mask length N and duty cycle ρ , there exist range-glint-ideal transmission masks yielding zero ARGI for constant modulus constellations, by *explicit construction*;
- We analyse the sidelobe performance of MASM, and prove that there exist transmission masks (including m -sequences) that are simultaneously ideal in the sense of range glint and sidelobe level, by *explicit construction*;
- We show that MASM can be applied as frame-level waveforms operating on the slow-time scale, and derive closed-form expressions characterising the relationship between slow-time and fast-time performance metrics.

The rest of this treatise is organised as follows. In Sec. II, we present the system model, including the transmit signal model, sensing reception processing and performance metrics. Based on these models, we analyse the range glint effect and formulate the range glint mitigation problem in Sec. III. We further analyse the sidelobe performance in Sec. IV, and discuss the application of MASM as slow-time coding in Sec. V. We verify and demonstrate the analytical results using numerical examples in Sec. VI, and finally conclude the treatise in Sec. VII.

Notations: The notations $\mathbf{0}_{M \times N}$, $\mathbf{1}_{M \times N}$, \mathbf{I}_m , $\mathbf{1}_m$, and $\mathbf{0}_m$ denote the $M \times N$ all-zero matrix, $M \times N$ all-one matrix, identity matrix of order m , m -dimensional all-one vector and m -dimensional all-zero vector, respectively. When they are clear from the context, the subscripts may be omitted. The notations $[\mathbf{A}]_{k,:}$, $[\mathbf{A}]_{:,l}$ and $[\mathbf{A}]_{i,j}$ denote the k -th row, the l -th column, and the (i, j) -th entry of matrix \mathbf{A} , respectively. $[\mathbf{x}]_{a:b}$ denotes the vector obtained by extracting the a -th to b -th entries from \mathbf{x} . $[\mathbf{m}]_i$ denotes the i -th entry of vector \mathbf{m} . $[\mathbf{x}; \mathbf{y}]$ and $[\mathbf{x}, \mathbf{y}]$ denote vertical and horizontal concatenation of vectors, respectively. The notation $|\mathbf{a}|$ denotes the entrywise

magnitude of \mathbf{a} , while $|\mathbf{a}|^2$ denotes the entrywise square of $|\mathbf{a}|$. $\mathbf{A} \odot \mathbf{B}$ denotes the Hadamard product. $\text{diag}(\mathbf{x})$ denotes the diagonal matrix constructed by placing \mathbf{x} on its main diagonal. $\|\cdot\|_p$ denotes the ℓ_p -norm of its argument, with $p = 2$ when the subscript is omitted. $\langle f, g \rangle$ denotes the inner product between f and g .

II. SYSTEM MODEL

Let us denote by T_c the symbol interval so that the bandwidth is $\frac{1}{T_c}$, and by NT_c the maximum distance at which we want to undertake sensing. As a consequence, the PRI coincides with NT_c . Let us also assume that we process a single PRI for sensing, so that the number of samples included in the processing interval is N .

A. Transmit Signal Model

The ISAC transmitter forms a data signal with duty cycle ρ , which means that it transmits the signal

$$x(t) = \sum_{i=-\infty}^{\infty} m_t(i)x_i\psi(t - iT_c), \quad (1)$$

where $m_t(i)$ is a periodic $(0, 1)$ -binary sequence with period N , referred to as the transmission mask, $\psi(t)$ denotes the pulse shaping filter in communication systems, and $\{x_i\}$ represents a zero-padded data sequence satisfying $x_i = 0$ for $m_t(i) = 0$, while for $m_t(i) = 1$ it holds that $x_i \in \mathcal{S}$, with $\mathcal{S} \subset \mathbb{C}$ being the coding alphabet (or constellation set). We assume that the communication symbols $x_i \neq 0$ are drawn from \mathcal{S} in an independently and identically distributed (i.i.d.) manner, satisfying the following assumptions.

Assumption 1 (Unit Power): We consider constellations having unit power, namely,

$$\mathbb{E}(|x|^2) = 1, \quad \forall x \in \mathcal{S}. \quad (2)$$

Assumption 1 normalises the power of the constellations, ensuring that they can be fairly compared against each other in terms of their sensing and communication performance.

Assumption 2 (Rotational Symmetry): We consider constellation having zero expectation and zero pseudo-variance, namely,

$$\mathbb{E}(x) = 0, \quad \mathbb{E}(x^2) = 0, \quad \forall x \in \mathcal{S}. \quad (3)$$

B. Sensing Reception Processing Model

If a single target is located at distance R from the transmitter, the transmitted signal would be reflected back to the receiver in a delayed manner, with the delay being $\tau_0 = \frac{2R}{c}$, whereby the noiseless signal impinging on the receive antenna would be

$$z_0(t) = x(t - \tau_0) = \sum_{i=-\infty}^{\infty} m_t(i)x_i\psi(t - \tau_0 - iT_c),$$

in keeping with (1). We do not consider the additive noise since it does not alter the reception process. The receiver may operate only during certain symbol intervals. To this end, we define the reception mask $m_r(i)$, which is also a periodic $(0, 1)$ -binary sequence with period N . The receiver undertakes the projections onto the basis $\{m_r(n)\psi(t - nT_c)\}$, thus yielding the observations

$$z_0(n) = \langle z(t), m_r(n)\psi(t - nT_c) \rangle. \quad (4)$$

For full-duplex systems, (4) is equivalent to the conventional matched filtering. For half-duplex systems, we have $m_r(i) = 1 - m_t(i)$, thereby the projection yields

$$z_0(n) = m_r(n) \sum_{i=-\infty}^{\infty} x_i m_t(i) \langle \psi(t - \tau_0 - iT_c), \psi(t - nT_c) \rangle.$$

If $\psi(\cdot)$ satisfies the Nyquist criterion with respect to T_c , and assuming $\tau_0 = kT_c$, then we obtain the sampled signal

$$z_k(n) = m_r(n) m_t(n - k) x_{n-k}, n \in \mathbb{Z}.$$

Since the processing interval is N , we actually have to process the finite-length sequence

$$\bar{z}_k(n) = z_k(n) R_N(n), R_Q(n) = \begin{cases} 1 & 0 \leq n \leq Q - 1 \\ 0 & \text{otherwise} \end{cases}$$

The transmitted sequence, on the other hand, reads

$$\bar{z}(n) = m_t(n) x_n$$

whereby the output of the correlator reads

$$\begin{aligned} r_{k,n} &= \bar{z}_k(n) * \bar{z}^*(-n) \\ &= \sum_{\ell=-\infty}^{\infty} m_r(\ell) m_t(\ell - k) m_t(\ell - n) x_{\ell-k} x_{\ell-n}^* R_N(\ell), \end{aligned}$$

namely

$$r_{k,n} = \sum_{\ell=0}^{N-1} m_r(\ell) m_t(\ell - k) m_t(\ell - n) x_{\ell-k} x_{\ell-n}^*. \quad (5)$$

Whenever it is more convenient, we may use the following vectorized notations:

$$\mathbf{m}_t = [m_t(0), \dots, m_t(N-1)]^T, \quad (6a)$$

$$\mathbf{m}_r = [m_r(0), \dots, m_r(N-1)]^T, \quad (6b)$$

$$\mathbf{x}_i = [x_{iN}, \dots, x_{(i+1)N-1}]^T, \quad (6c)$$

which amount to

$$\begin{aligned} r_{k,l} &= [\mathbf{0}_N; \mathbf{x}_0; \mathbf{0}_N]^H (\mathbf{I}_3 \otimes \mathbf{M}_t) \tilde{\mathbf{J}}_l^H (\mathbf{I}_3 \otimes \mathbf{M}_r) \tilde{\mathbf{J}}_k \\ &\quad \cdot (\mathbf{I}_3 \otimes \mathbf{M}_t) [\mathbf{x}_{-1}; \mathbf{x}_0; \mathbf{x}_1], \end{aligned} \quad (7)$$

as portrayed in Fig. 2, where $\mathbf{M}_t = \text{diag}(\mathbf{m}_t)$, $\mathbf{M}_r = \text{diag}(\mathbf{m}_r)$, and $\tilde{\mathbf{J}}_k$ denotes the n -th periodic shift matrix taking the following form

$$\tilde{\mathbf{J}}_k = \begin{bmatrix} \mathbf{0} & \mathbf{I}_{k \times k} \\ \mathbf{I}_{(3N-k) \times (3N-k)} & \mathbf{0} \end{bmatrix}. \quad (8)$$

We shall denote the i -th entry in \mathbf{m}_t and \mathbf{m}_r by $m_{t,i}$ and $m_{r,i}$, respectively. The duty cycle can then be expressed as

$$\rho = \frac{1}{N} \mathbf{1}^T \mathbf{m}_t. \quad (9)$$

C. Performance Metrics

The sensing and communication performance may be evaluated using metrics derived from the transmission mask and the corresponding range response. Next, we discuss several important performance metrics.

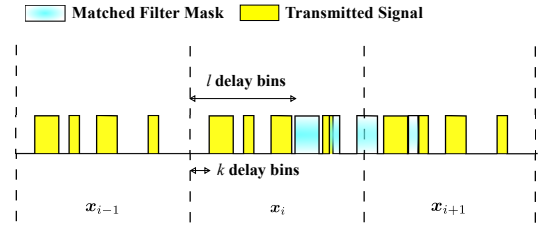


Fig. 2. Illustration of the reception processing in (7). We focus on the 0-th PRI \mathbf{x}_0 throughout the treatise, although all results also apply to other PRIs.

1) *Range glint*: The mainlobe level is often of interest, given by

$$r_{k,k} = \sum_{\ell=0}^{N-1} m_r(\ell) m_t(\ell - k) |x_{\ell-k}|^2, \quad (10)$$

which depicts the total received energy of an echo within the k -th delay bin. In the full-duplex case, the mainlobe level can simply be obtained as

$$r_{k,k} = \mathbf{x}_0^H \tilde{\mathbf{J}}_k^H \tilde{\mathbf{J}}_k \mathbf{x}_0 = \|\mathbf{x}_0\|_2^2,$$

which is constant with respect to k . Unfortunately, this is no longer the case for half-duplex systems. Such fluctuations of mainlobe levels across different delay bins would result in unexpected misdetections or false alarms, especially in multi-target sensing scenarios. In the rest of this treatise, we will refer to this phenomenon as the “range glint” effect of half-duplex systems.

Formally, we may define the range glint intensity (RGI) of the k -th range bin as

$$g_k(\mathbf{r}_m) = \left| r_{k,k} - \frac{1}{N-1} \sum_{l=1}^{N-1} r_{l,l} \right|^2, \quad (11)$$

for $k = 1, \dots, N-1$, where $\mathbf{r}_m = [r_{0,0}, \dots, r_{N-1,N-1}]^T$. Note that we do not consider the RGI at $k = 0$, since $r_{0,0} = 0$ holds for all half-duplex sensing systems, and hence any target within this range bin is undetectable (known as the blind range of half-duplex sensing systems). When the global range glint performance is considered, we may also define the averaged range glint intensity (ARGI) as follows

$$\bar{g}(\mathbf{r}_m) = \frac{1}{N-1} \sum_{k=1}^{N-1} |r_{k,k}|^2 - \left| \frac{1}{N-1} \sum_{l=1}^{N-1} r_{l,l} \right|^2. \quad (12)$$

A sensing signal with a low ARGI is thus desired for half-duplex sensing systems. For ISAC systems, since the communication symbols \mathbf{x}_i are random, one may wish to use the expected ARGI

$$\text{EARGI} = \mathbb{E}_{\mathbf{x}_0} \{ \bar{g}(\mathbf{r}_m) \}$$

to evaluate the performance of the mainlobe of the range response. We observe that the expected ARGI is in fact independent of the communication symbols, and hence applies to all PRIs (not limited to \mathbf{x}_0).

Remark 1 (ARGI as Conditional Variance): At this stage, let us elaborate on the physical implications of the aforementioned range glint metrics. In particular, the ARGI may be interpreted as the variance of mainlobe level across delay bins $k > 1$, given by

$$\bar{g}(\mathbf{r}_m) = \frac{1}{N-1} \sum_{k=1}^{N-1} \left| r_{k,k} - \frac{1}{N-1} \sum_{l=1}^{N-1} r_{l,l} \right|^2,$$

conditioned on a fixed realization of the communication symbols \mathbf{x}_0 . The RGI is thus a metric depicting the deviation of $r_{k,k}$ to the mean mainlobe level across all delay bins.

Note that ARG1 (and hence expected ARG1) has the following properties:

Proposition 1: It follows that

- 1) $\bar{g}(\mathbf{r}) = \bar{g}(-\mathbf{r})$;
- 2) $\bar{g}(\mathbf{r} + c\mathbf{1}) = \bar{g}(\mathbf{r})$, $\forall c \in \mathbb{R}$.

2) *Sidelobe level metrics:* The (squared) sidelobe levels $|r_{k,l}|^2$, $k \neq l$, are also useful. In particular, a widely applied performance criterion, the integrated sidelobe level (ISL), is defined based on the sidelobe levels as follows

$$\text{ISL}_k = \sum_{l \neq k} |r_{k,l}|^2, \quad (13)$$

where is independent of k for full-duplex systems. For conventional pulse radars, the ISL is also independent of k outside their blind ranges. For MASM systems, ISL is no longer the most suitable sidelobe performance metric, since it not only relies on k but also depends on the random data payload. To this end, in this treatise, we consider the average expected sidelobe level (AESL), which is averaged across all range bins, defined as

$$\text{AESL} = \sum_{k=1}^{N-1} \sum_{l>0, k \neq l} \mathbb{E}\{|r_{k,l}|^2\}. \quad (14)$$

In some scenarios, the peak sidelobe level is also useful. Thus we define the peak expected sidelobe level (PESL) as follows

$$\text{PESL} = \max_{k>0, l>0, l \neq k} \mathbb{E}\{|r_{k,l}|^2\}. \quad (15)$$

3) *Energy accumulation efficiency:* Since full-duplex systems transmit continuous waveforms, they typically accumulate echo energy more efficiently than half-duplex systems. Following this intuition, we define the energy accumulation efficiency as the ratio between the actual received echo energy and the received echo energy of a full-duplex system having identical configurations (including constellations, transmit power, frequency band, etc.) except for the transmission and reception masks, averaged across all delay bins, given by

$$\eta_S = \frac{\sum_{k=0}^{N-1} \mathbb{E}\{r_{k,k}\}}{N \mathbb{E}\{\|\mathbf{x}_i\|_2^2\}} = \frac{1}{N^2} \sum_{k=0}^{N-1} \mathbb{E}\{r_{k,k}\}. \quad (16)$$

Naturally, the energy accumulation efficiency of full-duplex systems is 1. For half-duplex systems, using the aforementioned assumptions (9) and (2), we have

$$\begin{aligned} \mathbb{E}\{r_{k,k}\} &= \mathbb{E}\left\{\left\|(\mathbf{I} - \mathbf{M}_t)\tilde{\mathbf{J}}_k \mathbf{M}_t \mathbf{x}_i\right\|_2^2\right\} \\ &= (\mathbf{1} - \mathbf{m}_t)^T \left(\tilde{\mathbf{J}}_k(\mathbf{m}_t \odot \mathbb{E}\{|\mathbf{x}_i|^2\})\right) \\ &= \rho N - \mathbf{m}_t^T \tilde{\mathbf{J}}_k \mathbf{m}_t. \end{aligned} \quad (17)$$

By rewriting the correlation $\{\mathbf{m}_t^T \tilde{\mathbf{J}}_k \mathbf{m}_t\}_{k=0}^{N-1}$ in the frequency domain, we further obtain

$$\mathbb{E}\{\mathbf{r}_m\} = \rho N \mathbf{1} - \sqrt{N} \mathbf{F}^H |\mathbf{F} \mathbf{m}_t|^2, \quad (18)$$

where

$$\mathbf{F} = \frac{1}{\sqrt{N}} \begin{bmatrix} \omega_N^{0,0} & \omega_N^{0,1} & \dots & \omega_N^{0,(N-1)} \\ \omega_N^{1,0} & \omega_N^{1,1} & \dots & \omega_N^{1,(N-1)} \\ \vdots & \vdots & \ddots & \vdots \\ \omega_N^{(N-1),0} & \omega_N^{(N-1),1} & \dots & \omega_N^{(N-1),(N-1)} \end{bmatrix}$$

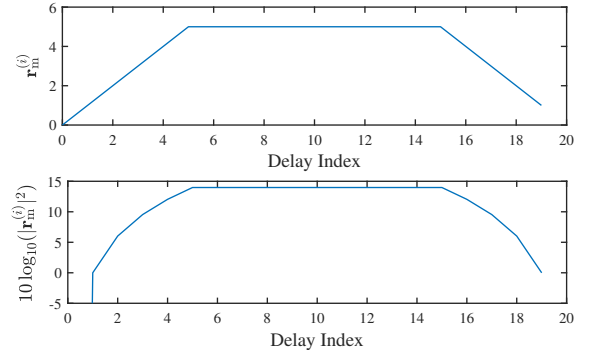


Fig. 3. Illustration of the range glint effect of conventional pulse radars. Trapezoidal \mathbf{r}_m 's suffer from severe range glint across many range bins.

denotes the unitary matrix representing the discrete Fourier transform, with $\omega_N = \exp(-2\pi i/N)$. Therefore

$$\begin{aligned} \mathbf{1}^T \mathbb{E}\{\mathbf{r}_m\} &= \rho N^2 - \sqrt{N} \mathbf{1}^T \mathbf{F}^H |\mathbf{F} \mathbf{m}_t|^2 \\ &= \rho N^2 - N [1; \mathbf{0}_{N-1}]^T |\mathbf{F} \mathbf{m}_t|^2 \\ &= \rho N^2 - N |\mathbf{f}_1^T \mathbf{m}_t|^2 \\ &= \rho N^2 - \rho^2 N^2. \end{aligned}$$

where $\mathbf{f}_1^T = \frac{1}{\sqrt{N}} \mathbf{1}^T$ is the first row of \mathbf{F} . We may then conclude that

$$\eta_S = \frac{\rho N^2 - \rho^2 N^2}{N^2} = \rho(1 - \rho).$$

It is clear that when $\rho = 0.5$, the energy accumulation efficiency achieves its maximum value 0.25. Systems with higher energy accumulation efficiency can achieve a larger signal-to-noise ratio (SNR) under the same peak power constraint.

4) *Communication throughput:* From the perspective of the communication system, the ISAC signal should convey as much information as possible. The communication throughput of MASM systems can be computed as

$$T = \frac{1}{N} \mathbf{1}^T \mathbf{m}_t \log_2(|\mathcal{S}|) = \rho \log_2(|\mathcal{S}|) \quad (19)$$

for each channel use [26], where ρ is the duty cycle and $|\mathcal{S}|$ represents the order of the constellation. In light of this, given a fixed constellation, the communication throughput constraint can be simplified as a duty cycle constraint.

III. THE RANGE GLINT EFFECT: ANALYSIS AND MITIGATION

A. Range Glint of Conventional Pulse Radars

Let us commence with a range glint analysis of conventional pulse radar waveforms, which will in turn motivate the design of MASM. A typical pulse radar has a continuous transmission interval in each PRI, namely

$$\mathbf{m}_t = [\mathbf{1}_{\rho N}; \mathbf{0}_{(1-\rho)N}]. \quad (20)$$

The waveforms of pulse radars are typically constant modulus, deterministic signals, with linear frequency modulated signals being a representative example. For these waveforms, according to (17), the mainlobe of the range response can be written as

$$r_{k,k} = \mathbb{E}\{r_{k,k}\} = (\mathbf{1} - \mathbf{m}_t)^T \tilde{\mathbf{J}}_k \mathbf{m}_t. \quad (21)$$

It then follows that

$$\mathbf{r}_m = \rho N \mathbf{1} - \sqrt{N} \mathbf{F}^H |\mathbf{F} \mathbf{m}_t|^2. \quad (22)$$

Note that $\sqrt{N}\mathbf{F}^H|\mathbf{F}\mathbf{m}_t|^2$ is in fact the periodical autocorrelation function (ACF) of \mathbf{m}_t . This suggests that the significance of the range glint effect may be intuitively depicted by the flatness of the ACF. For continuous transmission masks taking the form of (20), the periodical ACF is the convolution of a boxcar function with itself, and hence has a triangular shape. Consequently, as a function of m , \mathbf{r}_m has a trapezoidal shape, as illustrated in Fig. 3. The regions (especially the one containing the zeroth delay bin) in which \mathbf{r}_m does not take its maximum value ρN are typically referred to as the *blind range* in the radar literature [21, Sec. 1.5]. In the context of the range glint effect, the blind range may be defined as a set \mathcal{B} of delay bins in which the system suffers from severe range glint, in the sense that

$$|r_{k,k}|^2 \leq \frac{c_{\text{th}}}{N} \sum_{l=1}^N |r_{l,l}|^2, \quad \forall k \in \mathcal{B},$$

where $c_{\text{th}} < 1$ is a threshold depicting the system's tolerance of range glint. Apparently, for conventional pulse radars, the blind range expands as the duty cycle ρ increases, thereby raising a tradeoff between the target sensing capability and communication throughput.

B. Range Glint Mitigation Problem

Naturally, we would expect that a more favourable sensing-communication tradeoff can be achievable by using transmission masks suffering from milder range glint, or quantitatively, having a smaller ARGJ. This requirement may be formulated as the following optimisation problem

$$\min_{\mathbf{m}_t \in \{0,1\}^N} \bar{g}(\mathbf{r}_m), \quad (23a)$$

$$\text{s.t. } \mathbf{1}^T \mathbf{m}_t = \rho N. \quad (23b)$$

1) *Deterministic Constant Modulus Waveforms*: For pulse radars employing deterministic, constant modulus signals, we have the following result.

Proposition 2: The ARGJ of deterministic constant modulus signals can be computed as

$$\bar{g}(\mathbf{r}_m) = \frac{N}{N-1} \|\mathbf{F}\mathbf{m}_t\|_4^4 - \frac{\rho^2 N^3 (\rho^2 N - 2\rho + 1)}{(N-1)^2}. \quad (24)$$

Proof: Please refer to Appendix I-A. ■

Proposition 2 implies that the objective function in the optimisation problem (23) can be replaced with the simpler term $\|\mathbf{F}\mathbf{m}_t\|_4^4$. Note that $\|\mathbf{F}\mathbf{m}_t\|_4^4 = \|\mathbf{F}\mathbf{m}_t\|_2^4$, where $|\mathbf{F}\mathbf{m}_t|^2$ is the power spectrum of \mathbf{m}_t . A closely related quantity is the power spectral variance of \mathbf{m}_t given by

$$\text{PSV}(\mathbf{m}_t) := \frac{1}{N} \mathbf{1}^T \left(|\mathbf{F}\mathbf{m}_t|^2 - \frac{1}{N} \mathbf{1}^T |\mathbf{F}\mathbf{m}_t|^2 \right)^2, \quad (25)$$

which can be rewritten as

$$\text{PSV}(\mathbf{m}_t) = \frac{1}{N} \|\mathbf{F}\mathbf{m}_t\|_4^4 - \rho^2.$$

Thus we may now conclude that designing constant modulus low-ARGJ transmission masks is equivalent to minimizing the power spectral variance of the mask. In other words, transmission masks having flat power spectra will suffer less from the range glint effect.

2) *Data Payload Signals*: In general, for ISAC systems, we have to account for non-constant modulus transmit signals, modulated by random data payload via the orthonormal transformation \mathbf{U} . Consequently, the expected ARGJ would depend on the constellations of the data payload signal, detailed as follows.

Proposition 3 (Expected ARGJ of data payload signals): The expected ARGJ of data payload signals can be expressed as

$$\begin{aligned} \mathbb{E}_{\mathbf{x}_i} \{\bar{g}(\mathbf{r}_m)\} &= \frac{N}{N-1} \|\mathbf{F}\mathbf{m}_t\|_4^4 - \frac{\rho^2 N^3}{(N-1)^2} (\rho^2 N - 2\rho + 1) \\ &\quad + (\mu_4 - 1) \cdot \frac{\rho(1-\rho)N^2}{(N-1)^2} (\rho N - 1). \end{aligned} \quad (26)$$

Proof: Please refer to Appendix I-B. ■

We may now conclude that for data payload signals with generic constellations, the objective function in (23) can be replaced with the ℓ_4 norm $\|\mathbf{F}\mathbf{m}_t\|_4$, since the constellation-dependent term is independent of \mathbf{m}_t .

Remark 2: Since $1 - \rho \geq 0$ and $\rho N - 1 \geq 0$ hold for all transmission masks, we see that the expected ARGJ increases with μ_4 , with constant modulus constellations being the optimum. This suggests a deterministic-random tradeoff (DRT): sensing tasks favor constant modulus constellations, whereas the communication task would favor constellations having larger μ_4 for more efficient information transmission.

C. Solutions to the range glint mitigation problem

The range glint mitigation problem can now be written as

$$\min_{\mathbf{m}_t \in \{0,1\}^N} \|\mathbf{F}\mathbf{m}_t\|_4^4, \quad (27a)$$

$$\text{s.t. } \mathbf{1}^T \mathbf{m}_t = \rho N. \quad (27b)$$

This is a nonlinear integer programming problem that typically does not admit efficient algorithms yielding exact solutions. In the range of $N < 30$, it is possible to obtain the optimal solution by means of an exhaustive search. For large- N scenarios, in general, one may obtain suboptimal solutions by using the branch and bound approach [27], which can be relatively efficient in this context since the objective function $\|\mathbf{F}\mathbf{m}_t\|_4^4$ is convex in \mathbf{m}_t .

Fortunately, we may obtain optimal solutions under certain configurations of ρ and N . In particular, these solutions are not only optimal, but also *ideal* in the sense that their expected ARGJ can be exactly zero for constant modulus constellations, and hence can be computed as follows:

$$\mathbb{E}_{\mathbf{x}_0} \{\bar{g}(\mathbf{r}_m)\} = (\mu_4 - 1) \cdot \frac{\rho(1-\rho)N^2}{(N-1)^2} (\rho N - 1). \quad (28)$$

In what follows, we shall refer to these \mathbf{m}_t 's as *range-glint-ideal transmission masks*, and refer to the corresponding data payload signals as *range-glint-ideal data payload signals*. Let us denote

$$a_k := \mathbb{E}\{r_{k,k}\} = (\mathbf{1} - \mathbf{m}_t)^T \tilde{\mathbf{J}}_k \mathbf{m}_t,$$

and $\mathbf{a} = [a_0, \dots, a_{N-1}]^T$, we have the following result.

Lemma 1: It holds that

$$\begin{aligned} &\frac{N}{N-1} \|\mathbf{F}\mathbf{m}_t\|_4^4 - \frac{\rho^2 N^3}{(N-1)^2} (\rho^2 N - 2\rho + 1) \\ &= \frac{1}{N-1} \sum_{k=1}^{N-1} \left(a_k - \frac{1}{N-1} \sum_{l=1}^{N-1} a_l \right)^2. \end{aligned} \quad (29)$$

TABLE I

THE SCALING OF THE RATIO BETWEEN THE EXPECTED ARG I AND THE AVERAGE EXPECTED MAINLOBE LEVEL (AVERAGED OVER DELAY BINS), WITH RESPECT TO N , FOR DIFFERENT DATA PAYLOAD SIGNALS.

	Constant modulus constellations	Generic constellations
Conventional pulse	$O(1)$	$O(1)$
Random transmission masks	$O(1/N)$	$O(1/N)$
Range-glint-ideal transmission masks	0	$O(1/N)$

Proof: According to Proposition 2, we have

$$\bar{g}(\mathbf{a}) = \frac{N}{N-1} \|\mathbf{F}\mathbf{m}_t\|_4^4 - \frac{\rho^2 N^3}{(N-1)^2} (\rho^2 N - 2\rho + 1). \quad (30)$$

But from (12), we obtain

$$\begin{aligned} \bar{g}(\mathbf{a}) &= \frac{1}{N-1} \sum_{k=1}^{N-1} a_k^2 - \left(\frac{1}{N-1} \sum_{l=1}^{N-1} a_l \right)^2 \\ &= \frac{1}{N-1} \sum_{k=1}^{N-1} \left(a_k - \frac{1}{N-1} \sum_{l=1}^{N-1} a_l \right)^2. \end{aligned} \quad (31)$$

Combining (30) with (31) we obtain (29). ■

For conventional continuous pulses, the right-hand side of (29) is on the order of $O(N^2)$. For random transmission masks drawn from $\{0, 1\}^N$, we have the following result.

Proposition 4 (Expected ARG I of random masks): For random transmission masks whose entries are sampled from i.i.d. Bernoulli distributions $\text{Bern}(\rho)$, the expected ARG I (over both transmission masks and communication symbols) is given by

$$\begin{aligned} \mathbb{E}\{\bar{g}(\mathbf{r}_m)\} &= \frac{\rho^2(1-\rho)^2 N(N-2)}{N-1} \\ &+ (\mu_4 - 1) \cdot \frac{\rho(1-\rho)N^2}{(N-1)^2} (\rho N - 1). \end{aligned} \quad (32)$$

Proof: Please refer to Appendix I-C. ■

Now note that the average expected mainlobe level is in the order of $O(N^2)$. This suggests that as N increases, data payload signals modulated on conventional pulses would have a roughly constant ARG I-to-mainlobe-level ratio, but for random transmission masks and range-glint-ideal data payload signals this ratio will be vanishing. Our observations are summarised in Table I.

To find range-glint-ideal solutions, let us first note a simple relationship between the periodic ACF of $(0, 1)$ -binary sequences and $(+1, -1)$ -binary sequences:

Lemma 2: Denote the periodic ACF of a $(0, 1)$ -binary sequence \mathbf{x} as \mathbf{r}_x . Using the transformation $\mathbf{y} = \mathbf{1} - 2\mathbf{x}$ one may obtain a $(+1, -1)$ -binary sequence. It turns out that the periodic ACF \mathbf{r}_y of \mathbf{y} satisfies

$$\mathbf{r}_y = N(1 - 4\rho) + 4\mathbf{r}_x. \quad (33)$$

Proof: The entries of \mathbf{r}_y can be computed as

$$\begin{aligned} [\mathbf{r}_y]_k &= (\mathbf{1} - 2\mathbf{x})^T \tilde{\mathbf{J}}_{k-1} (\mathbf{1} - 2\mathbf{x}) \\ &= N + 4\mathbf{x}^T \tilde{\mathbf{J}}_{k-1} \mathbf{x} - 4\mathbf{x}^T \tilde{\mathbf{J}}_{k-1} \mathbf{1} \\ &= N - 4\rho N + 4[\mathbf{r}_x]_k, \end{aligned}$$

where $[\mathbf{r}_x]_k$ denotes the k -th entry of \mathbf{r}_x , thus yielding (33). ■

Lemma 2 implies that the ARG I of a $(0, 1)$ -binary sequence (e.g., \mathbf{m}_t) equals to that of the corresponding $(+1, -1)$ -binary sequence. In light of this, we may find range-glint-ideal transmission masks by resorting to the classical theory

of $(+1, -1)$ -binary sequence design aiming for finding sequences associated with so-called “two-level ACFs”, whose ACF sidelobes are identical [28].¹ From the definition of RGI (11), it is clear that transmission masks \mathbf{m}_t having two-level ACFs would have zero RGI for all $k > 0$. A well-known class of sequences belonging to this kind is the m -sequences, whose ACF takes the value of N at the mainlobe, with all sidelobes being equal to -1 . The Barker codes widely used in the radar literature also satisfy the “two-level ACF” condition. However, all known Barker codes are rather short ($N \leq 13$), making them less suitable for our purpose.

In general, binary sequences having two-level ACFs are known to be equivalent to the *cyclic difference sets (CDSs)* over finite abelian groups [29]. Formally, a (ν, k, λ) -CDS is a subset \mathcal{C} of \mathbb{Z}_ν , satisfying $|\mathcal{C}| = k$ and

$$|(w \oplus \mathcal{C}) \cap \mathcal{C}| = \lambda, \quad \forall w \in \mathbb{Z}_\nu,$$

where $w \oplus \mathcal{C} := \{(w + n) \bmod \nu | n \in \mathcal{C}\}$. In the context of transmission mask design, we have $\nu = N$, $k = \rho N$, and $\lambda = \rho N - r_{l,l}$, $\forall l$. A range-glint-ideal transmission mask $\mathbf{m}_t \in \{0, 1\}^N$ can be characterised using its associated CDS \mathcal{C} in the following manner

$$m_{t,i} = \begin{cases} 1, & i - 1 \in \mathcal{C}; \\ 0, & i - 1 \notin \mathcal{C}. \end{cases} \quad (34)$$

A large number of CDSs has been found, as summarised in [30]. Some notable subclasses include GMW CDSs [31], Paley CDSs [32], and Singer CDSs [33]. In particular, Singer CDSs is especially suitable for our purpose, as detailed later in Sec. IV.

IV. SIDELOBE ANALYSIS

In this section, we consider the sidelobe of the range response.

A. Average Expected Sidelobe

For unmodulated masks (i.e., satisfying $\mathbf{x}_i \propto \mathbf{1}$), we may construct a matrix \mathbf{R} given by

$$\mathbf{R} = N \mathbf{F}^H \text{diag}(\mathbf{F}^* \mathbf{m}_t^*) \mathbf{F} (\mathbf{I} - \mathbf{M}_t) \mathbf{F}^H \text{diag}(\mathbf{F} \mathbf{m}_t) \mathbf{F}, \quad (35)$$

which satisfies $[\mathbf{R}]_{k,l} = r_{k,l}$, and thus the off-diagonal entries of \mathbf{R} correspond to the sidelobes, while diagonal entries correspond to the mainlobes at different delay bins. For data payload signals, we have the following result.

Proposition 5: The expected sidelobe levels of data payload signals satisfy

$$\mathbb{E}\{|r_{k,l}|^2\} = [\mathbf{R}]_{k,l}, \quad \forall k \neq l. \quad (36)$$

Proof: Please refer to Appendix II-A. ■

¹Please be aware that the “sidelobe” in this context is the sidelobe of the ACF, rather than the sidelobe levels $|r_{k,l}|^2$, $k \neq l$ of the range response.

TABLE II
EXAMPLES OF IDEAL TRANSMISSION MASKS ASSOCIATED WITH SINGER CDSs.

Projective Space	N	ρ	CDS	Remark
$\mathbb{P}\mathbb{G}(2, 2)$	7	3/7	{0, 1, 3}	m -sequence, Barker code
$\mathbb{P}\mathbb{G}(2, 3)$	13	4/13	{0, 1, 4, 6}	Barker code
$\mathbb{P}\mathbb{G}(3, 2)$	15	7/15	{0, 1, 2, 7, 9, 12, 13}	m -sequence
$\mathbb{P}\mathbb{G}(3, 3)$	40	13/40	{0, 1, 2, 4, 5, 8, 13, 14, 17, 19, 24, 26, 34}	

Proposition 5 suggests a quadratic sidelobe level reduction of random data payload signals over pure masks. Next, we present a simple but important characteristic of the AESL.

Proposition 6 (Constant AESL): Given the parameters N and ρ , the AESL of data payload signals is *independent* of the transmission mask \mathbf{m}_t . In particular, we have

$$\frac{\sum_{k=1}^{N-1} \sum_{l>0, l \neq k} \mathbb{E}\{|r_{k,l}|^2\}}{(N-1)(N-2)} = \frac{\rho(1-\rho)N^2(\rho N-1)}{(N-1)(N-2)}, \quad (37)$$

where the average is taken over all sidelobes besides those in the blind range (i.e., $k=0$ or $l=0$).

Proof: Please refer to Appendix II-B. ■

B. Peak Expected Sidelobe

Proposition 6 suggests that expected ISL is not an appropriate sidelobe performance metric for designing the transmission mask \mathbf{m}_t . In this subsection, we investigate the PESL characteristics of MASM signals. The transmission mask design problem minimizing the PESL can be formulated using terminologies similar to those in the CDS formalism, as follows:

$$\min_{\mathcal{C}} \max_{k>0, l>0, l \neq k} |(k \oplus \mathcal{C}) \cap (l \oplus \mathcal{C})| - |(k \oplus \mathcal{C}) \cap (l \oplus \mathcal{C}) \cap \mathcal{C}|, \quad (38a)$$

$$\text{s.t. } |\mathcal{C}| = \rho N, \mathcal{C} \subseteq \mathbb{Z}_N, \quad (38b)$$

with the transmission mask being the indicator function of the set \mathcal{C} , i.e., $m_{t,i} = \mathbb{I}\{i+1 \in \mathcal{C}\}$. For range-glint-ideal transmission masks, the term $|(k \oplus \mathcal{C}) \cap (l \oplus \mathcal{C})|$ is a constant according to the definition of CDSs, and hence the PESL minimisation problem can be simplified as

$$\max_{\mathcal{C}} \min_{k>0, l>0, l \neq k} |(k \oplus \mathcal{C}) \cap (l \oplus \mathcal{C}) \cap \mathcal{C}|, \quad (39a)$$

$$\text{s.t. } |\mathcal{C}| = \rho N, \mathcal{C} \subseteq \mathbb{Z}_N. \quad (39b)$$

In general, the problems (38) and (39) do not admit efficient and exact solutions except for small- N cases. Similar to the discussion of range glint minimisation problem, one may then be interested in the existence and constructions of PESL-ideal, or even simultaneously PESL-ideal and range-glint-ideal, transmission masks, under certain configurations of (N, ρ) . To this end, we should first concretise the concept of PESL-ideal transmission masks by finding an achievable lower bound for PESL. Using Proposition 6, the following lower bound on the PESL can be obtained straightforwardly.

Corollary 1 (Ideal PESL): For any transmission mask $\mathbf{m}_t \in \{0, 1\}^N$ satisfying $\mathbf{1}^T \mathbf{m}_t = \rho N$, the PESL is lower bounded by

$$\max_{k>0, l>0, l \neq k} \mathbb{E}\{|r_{k,l}|^2\} \geq \left\lceil \frac{\rho(1-\rho)N^2(\rho N-1)}{(N-1)(N-2)} \right\rceil. \quad (40)$$

Proof: Apparently, PESL is no smaller than the AESL, namely we have

$$\max_{k>0, l>0, l \neq k} \mathbb{E}\{|r_{k,l}|^2\} \geq \frac{\rho(1-\rho)N^2(\rho N-1)}{(N-1)(N-2)}.$$

Now note that all entries $[\mathbf{R}]_{k,l}$ are integers, thereby the result (40) follows from (36). ■

Next we show that the lower bound (40) is achievable (and hence is tight) for certain pairs of (N, ρ) , by means of explicit construction. Moreover, these transmission masks are simultaneously PESL-ideal and range-glint-ideal.

Proposition 7 (Singer CDSs are ideal transmission masks): The transmission masks obtained by Singer's construction of CDSs [33] are simultaneously range-glint-ideal and PESL-ideal. To elaborate, a transmission mask \mathbf{m}_t , whose corresponding convolution operator given by

$$\mathbf{A} = \mathbf{F} \text{diag}(\mathbf{F} \mathbf{m}_t) \mathbf{F}^H = [\mathbf{m}_t; \tilde{\mathbf{J}}_1 \mathbf{m}_t; \dots; \tilde{\mathbf{J}}_{N-1} \mathbf{m}_t] \quad (41)$$

is one of the possible incidence matrices between the points and hyperplanes (i.e., $(n-1)$ -dimensional subspaces) in the finite projective space $\mathbb{P}\mathbb{G}(n, q)$ (where q is a power of prime) with $N = (q^{n+1} - 1)(q - 1)^{-1}$, is both range-glint-ideal and PESL-ideal. The duty cycles of such transmission masks are determined by n and q according to

$$\rho = \frac{q^n - 1}{N(q - 1)}. \quad (42)$$

Proof: Please refer to Appendix II-C. ■

Proposition 7 indicates that whenever the corresponding (N, ρ) pairs are acceptable, the Singer CDSs should be chosen as the transmission masks. The family of Singer CDSs incorporates all m -sequences and some Barker codes. A subset of Singer CDSs is summarised in Table II. Readers interested in a detailed characterisation of these CDSs are referred to [34].

C. Comparison with the Full-Duplex Scheme

Now that we have characterised the range response (including both mainlobes and sidelobes) of half-duplex transmission masks, we may compare their performance with full-duplex transmission schemes. According to [11], the expected periodic ACF sidelobe level of full-duplex transmission schemes is simply given by²

$$\mathbb{E}\{|r_{k,l}|^2\} = N, \forall k \neq l. \quad (43)$$

Their corresponding expected mainlobe level is

$$\mathbb{E}\{|r_{k,k}|^2\} = N^2 + (\mu_4 - 1)N, \forall k.$$

Thus the mainlobe-to-PESL ratio and the mainlobe-to-AESL ratio depicting target detection dynamic range are equal to each other for full-duplex schemes, given by

$$\frac{\mathbb{E}\{|r_{k,k}|^2\}}{\mathbb{E}\{|r_{k,l}|^2\}} = N + \mu_4 - 1, \forall k \neq l. \quad (44)$$

By contrast, for half-duplex schemes, AESL and PESL are not necessarily equal. Furthermore, the mainlobe-to-PESL ratio

²In fact, (43) is the expression for single-carrier full-duplex transmission schemes. We quote this formula for the fairness of comparison, since half-duplex schemes cannot easily apply other modulation bases due to their non-continuous temporal support.

and the mainlobe-to-AESL ratio are only appropriately applicable to range-glint-ideal transmission masks. In particular, the mainlobe-to-AESL ratio of range-glint-ideal transmission masks is given by

$$\frac{\mathbb{E}\{|r_{k,k}|^2\}}{\mathbb{E}\{|r_{k,l}|^2\}} = \frac{\rho(1-\rho)(N-1)(N-2)}{\rho N - 1} + (\mu_4 - 1) \cdot \frac{N-2}{N-1}, \quad \forall k \neq l, k > 0, l > 0. \quad (45)$$

As N tends to infinity, it follows that

$$\frac{\mathbb{E}\{|r_{k,k}|^2\}}{\mathbb{E}\{|r_{k,l}|^2\}} \sim (1-\rho)N + \mu_4 + 1, \quad \forall k \neq l, k > 0, l > 0. \quad (46)$$

The mainlobe-to-PESL ratio is in general smaller, but PESL-ideal transmission masks can achieve the upper bound given by (45), thereby the asymptotic behaviour (46) also applies.

Remark 3 (Throughput-Sidelobe-Interference Tradeoff): The asymptotic behaviour (46) suggests a communication-sensing performance tradeoff: The communication throughput is proportional to ρ , but the target detection dynamic range is asymptotically proportional to $(1-\rho)$. As a typical operating point, the m -sequences have roughly $\rho = 1/2$ for large N , which achieves a 50% communication throughput and a 3dB loss of sensing dynamic range compared to the full-duplex scheme. These performance degradations can be viewed as the cost paid to obtain SI-free long-range sensing capability.

V. MASM APPLIED IN SLOW TIME

In the aforementioned discussions, we have considered the transmission mask design in the fast time. Unfortunately, practical hardware may not be capable of supporting a sample-level switching rate between transmitting and receiving modes. To this end, in this section, we consider the slow-time transmission mask design problem. In particular, we confine ourselves to the transmission masks taking the following piecewise constant form:

$$\mathbf{m}_t = \tilde{\mathbf{m}}_t \otimes \mathbf{1}_T, \quad (47)$$

where $\tilde{\mathbf{m}}_t \in \{0, 1\}^L$ represents the slow-time transmission mask, while T denotes the number of fast-time samples contained in each slow-time symbol, satisfying $LT = N$. Similar to \mathbf{m}_t , we denote the i -th entry of $\tilde{\mathbf{m}}_t$ as $\tilde{m}_{t,i}$.

A. Range Glint Analysis

In the fast-time version of MASM, we defined the expected ARG I as a metric of range glint, which characterises the mainlobe variation outside the inevitable blind range $k = 0$. Due to the piecewise constant structure (47), slow-time coding-based transmission strategies would yield blind ranges approximately as large as T , namely the length of a sub-pulse, corresponding to the ‘‘ramping up’’ region in Fig. 3. In light of this, we define the expected partial RGI as

$$\text{EPRGI}_k(\mathcal{B}) = \mathbb{E}\left\{\left|r_{k,k} - \frac{1}{N - |\mathcal{B}|} \sum_{l \in \bar{\mathcal{B}}} r_{l,l}\right|^2\right\}, \quad (48)$$

where \mathcal{B} and $\bar{\mathcal{B}}$ denote the sample indices corresponding to the blind range and the complement of the blind range (relative to $\{1, 2, \dots, N\}$), respectively. Before analysing the range glint performance of the slow-time coding strategy, we first present a simplified expression for the expected partial RGI.

Lemma 3: The expected partial RGI can be expressed as

$$\begin{aligned} \text{EPRGI}_k(\mathcal{B}) &= \left(a_k - \frac{1}{N - |\mathcal{B}|} \sum_{l \in \bar{\mathcal{B}}} a_l\right)^2 + (\mu_4 - 1) \\ &\times \left[-a_k + \frac{2}{N - |\mathcal{B}|} \sum_{q \in \bar{\mathcal{B}}} b_{kq} + \frac{1}{(N - |\mathcal{B}|)^2}\right. \\ &\times \left.\sum_{p' \in \bar{\mathcal{B}}} \sum_{q' \in \bar{\mathcal{B}}} (a_{p'} - b_{p'q'})\right], \end{aligned} \quad (49)$$

where $a_k = \mathbf{1}^T[(\mathbf{1} - \mathbf{m}_t) \odot \tilde{\mathbf{J}}_k \mathbf{m}_t]$ denotes the cross-correlation between transmission and reception masks, and $b_{lp} = \mathbf{1}^T[(\mathbf{1} - \mathbf{m}_t) \odot \tilde{\mathbf{J}}_l \mathbf{m}_t \odot \tilde{\mathbf{J}}_{l-p} \mathbf{m}_t]$.

Proof: Please refer to Appendix I-D. \blacksquare

From Lemma 3 we may observe that, the first term on the right-hand side of (49) is on the order of $O(N^2)$, while the second term (containing the factor $(\mu_4 - 1)$) is on the order of $O(N)$. This resembles the decomposition discussed in Sec. III-C. We may then conclude that, the key to reducing the expected partial RGI is to suppress the fluctuation between a_k 's.

Remark 4: In particular, we may say that a slow-time transmission mask $\tilde{\mathbf{m}}_t$ is range-glint-ideal up to the first order, whenever it satisfies

$$a_k = \frac{1}{N - |\mathcal{B}|} \sum_{l \in \bar{\mathcal{B}}} a_l, \quad \forall k \in \bar{\mathcal{B}}. \quad (50)$$

For these transmission masks, the range glint outside the blind range can be exactly zero under constant modulus constellations, namely $\mu_4 = 1$.

Next, we give a simple characterisation of $\{a_i\}_{i=0}^{N-1}$ under the piecewise constant constraint (47).

Proposition 8: The mask cross-correlation sequence $\{a_i\}_{i=0}^{N-1}$ satisfies

$$a_{kT+l} = T\tilde{a}_k + l \cdot d_k, \quad (51)$$

where $k = 0, \dots, L-1$, $l = 0, \dots, T-1$, \tilde{a}_k is the slow-time mask cross-correlation sequence defined as $\tilde{a}_k = \mathbf{1}^T[(\mathbf{1} - \tilde{\mathbf{m}}_t) \odot \tilde{\mathbf{J}}_k \tilde{\mathbf{m}}_t]$, while d_k denotes the cyclic difference of \tilde{a}_k given by

$$d_k = \tilde{a}_{(k+1) \bmod N} - \tilde{a}_k.$$

Proof: Please refer to Appendix III-A. \blacksquare

Since $\tilde{a}_0 = 0$ holds for all slow-time transmission masks, it then follows from Proposition 8 that when $k = 0$, or $k = L$ and $l > 0$, a_{kT+l} would suffer from inevitable range glint. Therefore, we define the blind range of such transmission masks as

$$\mathcal{B} = \{0, \dots, T-1\} \cup \{(L-1)T+1, \dots, LT-1\}. \quad (52)$$

Observe that (52) coincide with the blind range of conventional pulse radars with pulse width T . However, such systems can only transmit T communication symbols in each PRI. By contrast, the proposed slow-time coding scheme significantly improves the communication throughput to ρLT symbols per PRI.

Another important insight provided by Proposition 8 is that, in order to guarantee the first-order range glint ideality depicted by (50), it suffices to ensure that

$$\tilde{a}_k = \frac{1}{L-1} \sum_{l=1}^{L-1} \tilde{a}_l, \quad \forall k = 1, \dots, L-1. \quad (53)$$

In other words, if $\tilde{\mathbf{m}}_t$ is range-glint-ideal when applied as an ordinary transmission mask, it is also range-glint-ideal up to the first order when used as a slow-time transmission mask. Therefore, our discussions and constructions of ideal transmission masks in the previous sections can also be applied to slow-time coding schemes.

B. Sidelobe Analysis

Compared to the range glint analysis, the sidelobe analysis of slow-time coding schemes is much simpler. In particular, the expression (36) for the expected sidelobe level is still applicable. The remaining task is to further simplify the expression of \mathbf{R} via exploiting the piecewise constant structure of \mathbf{m}_t . In fact, by applying similar arguments as those used in Proposition 8, we may obtain the following result.

Corollary 2: Define the slow-time sidelobe level as

$$\tilde{a}_{k,l} = \sum_{n=1}^N \tilde{m}_{t,n-l} \tilde{m}_{t,n-k} (1 - \tilde{m}_{t,n}).$$

The expected sidelobe level under the slow-time coding scheme can then be written as

$$\mathbb{E}\{|r_{k_1 T + l_1, k_2 T + l_2}|^2\} = T \tilde{a}_{k_1, k_2} + l_1 \cdot d_{k_1, k_2}^{(1)} + l_2 \cdot d_{k_1, k_2}^{(2)}, \quad (54)$$

for $k_1 T + l_1 \neq 0$ and $k_2 T + l_2 \neq 0$, where

$$\begin{aligned} d_{k_1, k_2}^{(1)} &= \tilde{a}_{(k_1+1) \bmod N, k_2} - \tilde{a}_{k_1, k_2}, \\ d_{k_1, k_2}^{(2)} &= \tilde{a}_{k_1, (k_2+1) \bmod N} - \tilde{a}_{k_1, k_2}. \end{aligned}$$

Proof: This result can be obtained by applying again the arguments used for proving Proposition 8, detailed in Appendix III-A. ■

Corollary 2 implies that, the aforementioned discussions in Sec. IV concerning average sidelobe levels and peak sidelobe levels can also be applied to slow-time coding schemes via (54). In light of this, Singer CDSs are also ideal slow-time transmission masks in the sense detailed in Proposition 7.

VI. NUMERICAL RESULTS

In this section, we verify and demonstrate the analytical results discussed in previous sections using numerical examples.

A. Fast-Time MASM

Let us first consider the range glint effect. In Fig. 4, the expected mainlobe levels (i.e., $\mathbb{E}\{|r_{k,k}|^2\}$) of MASM having different transmission masks, as well as that of the conventional pulse, are portrayed. We consider PSK constellations, thereby the expected mainlobe level is sufficient to characterise range glint (see Proposition 3). Observe that the range glint of the conventional pulse and MASM with random transmission mask is rather significant, which is unsatisfactory. The optimal $N = 22$, $\rho = 1/2$ transmission mask exhibits much weaker range glint, with only 5 delay bins deviating from the most likely mainlobe level. The configuration $N = 23$, $\rho = 11/23$ admits a range-glint-ideal transmission mask (the Paley CDS) whose expected mainlobe level is constant across all delay bins $0 < k \leq N - 1$.

To demonstrate the scaling laws given in Table I, the ARGJ-to-mainlobe ratios of MASM under various constellations and transmission masks are compared against that of the conventional pulse in Fig. 5. The ratio is defined as

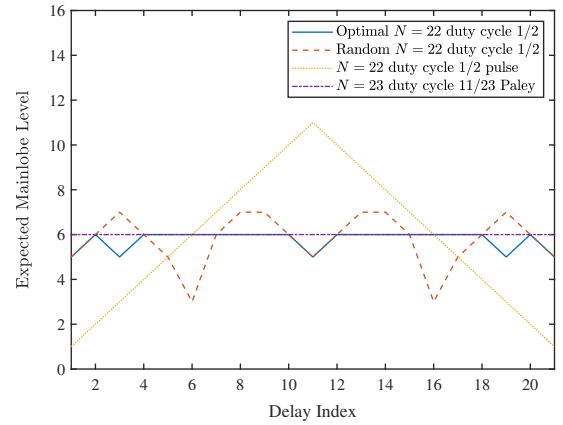


Fig. 4. The range glint of MASM under PSK constellations and different transmission masks, compared with the conventional pulse.

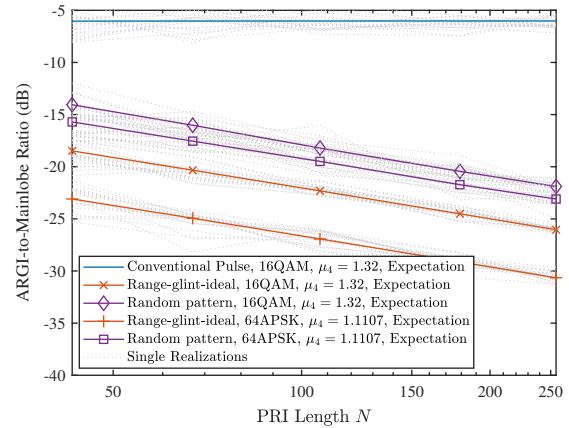


Fig. 5. The ARGJ-to-mainlobe ratio of MASM under various constellations and transmission masks, compared with the conventional pulse.

$N \cdot \text{ARGI} \cdot (\sum_{k=0}^{N-1} \mathbb{E}\{|r_{k,k}|^2\})^{-1}$. To ensure the fairness of comparison, all transmission masks have duty cycle approximately equal to 0.5. Observe that both random transmission masks and range-glnt-ideal masks exhibit $O(1/N)$ ARGJ-to-mainlobe ratios, while the conventional pulses have constant ARGJ-to-mainlobe ratios. Furthermore, the ratio reduces as m_4 decreases, as implied by Proposition 3.

Next, we investigate the sidelobe performance. In Fig. 6, the expected sidelobe levels of two different range-glnt-ideal $N = 63$, $\rho = 31/63$ transmission masks are portrayed. According to Proposition 6, the AESL is identical for both transmission masks, which equals $\frac{29760}{3782} \approx 7.869$. However, the Singer $\mathbb{P}\mathbb{G}(5, 2)$ sequence in Fig. 6a is PESL-ideal, whose expected sidelobe level is at most $\lceil 7.869 \rceil = 8$. By contrast, the GMW sequence in Fig. 6b has a PESL of 9.

Finally, let us verify and demonstrate the results in Sec. IV-C. In particular, we choose several range-glnt-ideal transmission masks with diverse (N, ρ) configurations, and plot their range response slices at mainlobe delay $k = 29$ in Fig. 7. The constellations are chosen to be QPSK. It is seen that the expected sidelobe levels can be fit well to the asymptotic reference sidelobe level of $1/[(1 - \rho)N]$, as depicted by (46).

B. Slow-Time MASM

In this subsection, we investigate the performance of MASM as a slow-time coding technique. The benchmark is the PRF staggering methods, with stagger ratios of 31 : 32 : 33, 25 :

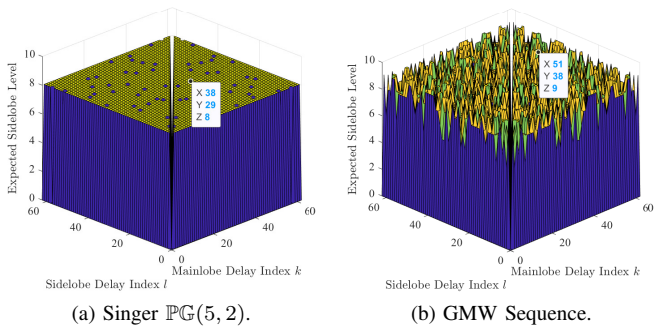


Fig. 6. The expected sidelobe levels of two different range-glint-ideal transmission masks, for which the (N, ρ) configuration is $N = 63$ and $\rho = 31/63$.

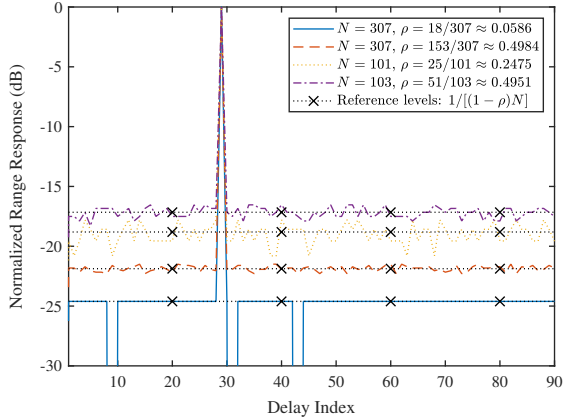


Fig. 7. Range response slices of MASM under different (N, ρ) configurations.

30 : 27 : 31 and 51 : 62 : 53 : 61 : 58, adopted from [35, Sec. 15.9]. The transmission mask for MASM is chosen to be the 63-point m -sequence, whose duty cycle is $31/63 \approx 0.492$. Each slow-time sample contains $T = 16$ symbols, resulting in $N = 1008$. To ensure that the total sequence lengths as well as the duty cycles of the considered methods are approximately equal to one another, we use the parameters in Table III for the PRF staggering methods.

We first consider the range glint effect. In Fig. 8, the slow-time MASM is compared with PRF staggering methods, in terms of the expected partial RGI, which is normalised in the following manner

$$\text{NEPRGI}_k(\mathcal{B}) = \frac{\mathbb{E}\left\{\left|r_{k,k} - \frac{1}{N-|\mathcal{B}|} \sum_{l \in \mathcal{B}} r_{l,l}\right|^2\right\}}{\mathbb{E}\{|r_{k,k}|^2\}}. \quad (55)$$

In this figure, we consider the 16QAM constellation. Observe that the range glint effect of MASM is much weaker than that of PRF staggering methods. This can be understood by revisiting (49), in which the first term on the right-hand side is zero for MASM. Therefore, the expected partial RGI of MASM is $O(N)$ times lower than that of PRF staggering methods.

Next, let us investigate the relationship between range glint and constellations, as portrayed in Fig. 9. Note that for MASM, the expected partial RGI is proportional to $(\mu_4 - 1)$. As seen in Fig. 9, the normalised expected partial RGI indeed decreases with the fourth moment μ_4 of the constellations. Moreover, the partial RGI averaged over 2000 random instances are in close proximity to their corresponding analytical expectations.

Finally, we consider the sidelobe performance of slow-time MASM. In Fig. 10, MASM is compared against the PRF staggering method having stagger ratio 51 : 62 : 63 : 61 : 58,

TABLE III
THE PARAMETERS USED FOR PRF STAGGERING METHODS.

Stagger ratio	No. of periods for each PRF	Pulse width	Duty cycle
31 : 32 : 33	11	16	0.500
25 : 30 : 27 : 31	11	14	0.496
51 : 62 : 53 : 61 : 58	4	28	0.491

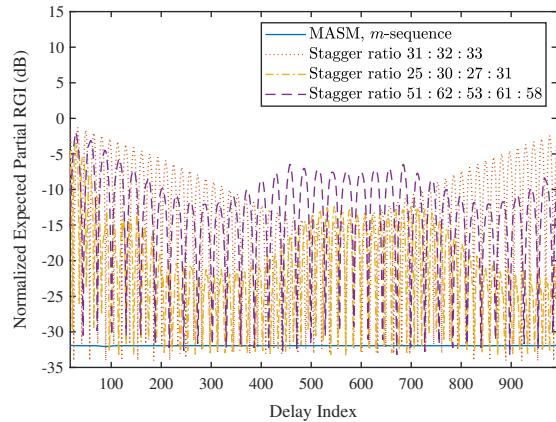


Fig. 8. The range glint of slow-time MASM compared with PRF staggering methods, under 16QAM constellations, measured by normalised expected partial RGI.

in terms of sidelobe level. The mainlobe is located at the 65-th delay bin. It is clear that the PESL of slow-time MASM is significantly lower than that of the PRF staggering method. Furthermore, the sidelobe levels at integer multiples of the slow-time sample period coincide with the (upsampled) sidelobe levels of the slow-time transmission mask, which corroborates Corollary 2.

VII. CONCLUSIONS

In this treatise, we have proposed MASM, a half-duplex ISAC transmission scheme avoiding the SI issue in long-range sensing. Compared to conventional pulse radar techniques and the PRF staggering techniques, MASM can mitigate the range glint effect, which characterises the range blindness, to a significantly lower level, while preserving large duty cycles ($\sim 50\%$). This empowers ISAC systems with high communication throughput and high energy accumulation efficiency. Furthermore, both range-glint-ideal and sidelobe-ideal transmission masks are constructed, which can be readily used in practical ISAC systems. Our hope is that MASM may be beneficially applied in future long-range ISAC scenarios, including low-altitude economy and autonomous driving.

APPENDIX I RANGE GLINT ANALYSIS

A. Proof of Proposition 2

Proof: The ARGJ can be expressed as

$$\begin{aligned} \bar{g}(\mathbf{r}_m) &= \frac{1}{N-1} \sum_{k=1}^{N-1} |r_{k,k}|^2 - \left| \frac{1}{N-1} \sum_{l=1}^{N-1} r_{l,l} \right|^2 \\ &= \frac{N}{N-1} \left[\|\mathbf{F}\mathbf{m}_t\|_4^4 - \frac{1}{N} (\mathbf{1}^T |\mathbf{F}\mathbf{m}_t|^2)^2 \right] \\ &\quad - \frac{N^2}{(N-1)^2} \left(\rho^2 N - \frac{1}{N} \mathbf{1}^T |\mathbf{F}\mathbf{m}_t|^2 \right)^2. \end{aligned} \quad (56)$$

Note that $\rho^2 N$ is constant with respect to \mathbf{m}_t . Using $\mathbf{1}^T |\mathbf{F}\mathbf{m}_t|^2 = \|\mathbf{m}_t\|_2^2$, we may rearrange the expression

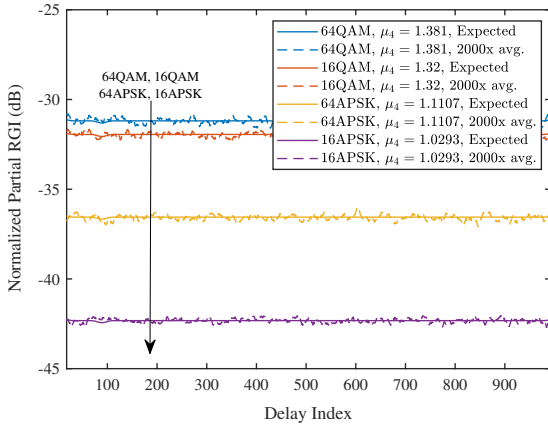


Fig. 9. The averaged and expected partial RGI of MASM under different constellations.

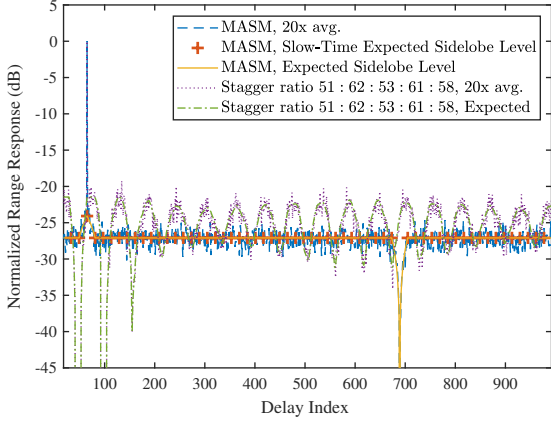


Fig. 10. The averaged and expected sidelobe level of MASM compared with that of PRF staggering methods.

of $\bar{g}(\mathbf{r}_m)$ by separating the terms containing \mathbf{m}_t from the constants, as follows:

$$\begin{aligned} \bar{g}(\mathbf{r}_m) &= \frac{N}{N-1} \|\mathbf{F}\mathbf{m}_t\|_4^4 - \frac{1}{N-1} \|\mathbf{m}_t\|_2^4 - \frac{\rho^4 N^4}{(N-1)^2} \\ &\quad + \frac{2\rho^2 N^2}{(N-1)^2} \|\mathbf{m}_t\|_2^2 - \frac{1}{(N-1)^2} \|\mathbf{m}_t\|_4^4 \\ &= \frac{N}{N-1} \|\mathbf{F}\mathbf{m}_t\|_4^4 - \frac{\rho^2 N^3 (\rho^2 N - 2\rho + 1)}{(N-1)^2}, \end{aligned} \quad (57)$$

which completes the proof. \blacksquare

B. Proof of Proposition 3

Proof: According to (10), we have

$$r_{k,k} = \left\| (\mathbf{1} - \mathbf{m}_t) \odot \left[\tilde{\mathbf{J}}_k(\mathbf{m}_t \odot \mathbf{x}_i) \right] \right\|_2^2.$$

Thereby the generic \mathbf{r}_m for half-duplex ISAC systems can be expressed as

$$\begin{aligned} \mathbf{r}_m &= \sqrt{N} \mathbf{F}^H \left[(\mathbf{F} \mathbf{m}_t \odot \mathbf{x}_i)^* \odot \mathbf{F}(\mathbf{1} - \mathbf{m}_t) \right] \\ &= -\sqrt{N} \mathbf{F}^H \left[(\mathbf{F}(\mathbf{m}_t \odot \mathbf{x}_i))^* \odot \mathbf{F}\mathbf{m}_t \right] \\ &\quad + \mathbf{1}^T (\mathbf{m}_t \odot \mathbf{x}_i)^2 \mathbf{1}. \end{aligned} \quad (58)$$

According to Proposition 1, the ARG I can be alternatively expressed as $\bar{g}(\mathbf{r}_m) = \bar{g}(\tilde{\mathbf{r}}_m)$, where

$$\tilde{\mathbf{r}}_m = \sqrt{N} \mathbf{F}^H \left[(\mathbf{F}(\mathbf{m}_t \odot \mathbf{x}_i))^* \odot \mathbf{F}\mathbf{m}_t \right].$$

This leads to a simpler form of the ARG I:

$$\begin{aligned} \bar{g}(\mathbf{r}_m) &= \frac{N}{N-1} \left[\|\mathbf{F}^*(\mathbf{m}_t \odot \mathbf{x}_i)^* \odot \mathbf{F}\mathbf{m}_t\|_2^2 \right. \\ &\quad \left. - \frac{1}{N} \left[\mathbf{1}^T \left((\mathbf{F}^*(\mathbf{m}_t \odot \mathbf{x}_i)^* \odot \mathbf{F}\mathbf{m}_t) \right)^2 \right] \right. \\ &\quad \left. - \frac{N^2}{(N-1)^2} \left(\rho \mathbf{1}^T (\mathbf{m}_t \odot \mathbf{x}_i)^2 \right) \right. \\ &\quad \left. - \frac{1}{N} \mathbf{1}^T \left((\mathbf{F}^*(\mathbf{m}_t \odot \mathbf{x}_i)^* \odot \mathbf{F}\mathbf{m}_t) \right)^2 \right]. \end{aligned}$$

The expectations of the terms constituting ARG I are as follows

$$\begin{aligned} &\mathbb{E} \left\{ \|\mathbf{F}^*(\mathbf{m}_t \odot \mathbf{x}_i)^* \odot \mathbf{F}\mathbf{m}_t\|_2^2 \right\} \\ &= \mathbf{1}^T \left(\mathbb{E} \left\{ \left| \mathbf{F}(\mathbf{m}_t \odot \mathbf{x}_i)^2 \right|^2 \right\} \odot |\mathbf{F}\mathbf{m}_t|^2 \right) \\ &= \sum_{n=1}^N |\mathbf{f}_n^T \mathbf{m}_t|^2 \mathbf{f}_n^H \mathbf{M}_t \mathbf{S} \mathbf{M}_t \mathbf{f}_n, \end{aligned} \quad (59)$$

where $\mathbf{S} := \mathbb{E} \{ |\mathbf{x}_i|^2 |\mathbf{x}_i|^{2T} \}$, \mathbf{f}_n denotes the transpose of the n -th row of \mathbf{F} ,

$$\mathbb{E} \left\{ \left[\mathbf{1}^T (\mathbf{m}_t \odot \mathbf{x}_i)^2 \right]^2 \right\} = \mathbf{m}_t^T \mathbf{S} \mathbf{m}_t,$$

$$\mathbb{E} \left\{ \left[\mathbf{1}^T \left((\mathbf{F}^*(\mathbf{m}_t \odot \mathbf{x}_i)^* \odot \mathbf{F}\mathbf{m}_t) \right)^2 \right] \right\} = \mathbf{m}_t^T \mathbf{S} \mathbf{m}_t,$$

and

$$\begin{aligned} &\mathbb{E} \left\{ \mathbf{1}^T (\mathbf{m}_t \odot \mathbf{x}_i)^2 \mathbf{1}^T \left((\mathbf{F}^*(\mathbf{m}_t \odot \mathbf{x}_i)^* \odot \mathbf{F}\mathbf{m}_t) \right) \right\} \\ &= \mathbf{m}_t^T \mathbf{S} \mathbf{m}_t. \end{aligned}$$

Thus we have

$$\begin{aligned} \mathbb{E}_{\mathbf{x}_0} \{ \bar{g}(\mathbf{r}_m) \} &= \frac{N}{N-1} \sum_{n=1}^N |\mathbf{f}_n^T \mathbf{m}_t|^2 \mathbf{f}_n^H \mathbf{M}_t \mathbf{S} \mathbf{M}_t \mathbf{f}_n \\ &\quad - \frac{1}{N-1} \mathbf{m}_t^H \mathbf{S} \mathbf{m}_t - \frac{\rho^2 N^2}{(N-1)^2} \mathbf{m}_t^H \mathbf{S} \mathbf{m}_t \\ &\quad - \frac{1}{(N-1)^2} \mathbf{m}_t^H \mathbf{S} \mathbf{m}_t + \frac{2\rho N}{(N-1)^2} \mathbf{m}_t^H \mathbf{S} \mathbf{m}_t \\ &= \frac{N}{N-1} \sum_{n=1}^N |\mathbf{f}_n^T \mathbf{m}_t|^2 \mathbf{f}_n^H \mathbf{M}_t \mathbf{S} \mathbf{M}_t \mathbf{f}_n \\ &\quad - \frac{N}{(N-1)^2} (\rho^2 N - 2\rho + 1) \mathbf{m}_t^H \mathbf{S} \mathbf{m}_t. \end{aligned} \quad (60)$$

We may now observe that the key to computing the expected ARG I is to obtain the matrix \mathbf{S} , for which we have

$$\mathbf{S} = \mathbf{1}\mathbf{1}^T + (\mu_4 - 1)\mathbf{I}, \quad (61)$$

where $\mu_4 = \mathbb{E} \{ |x|^4 \}$, $\forall x \in \mathcal{S}$. This implies (26). \blacksquare

C. Proof of Proposition 4

Proof: It suffices to compute the expectation of (29). Note that

$$a_k a_l = \sum_{p=1}^N \sum_{q=1}^N (1 - m_{t,p})(1 - m_{t,q}) m_{t,p-k} m_{t,q-l},$$

where $\overline{n-l}$ denotes the cyclic shift relation of $(n-l-1) \bmod N+1$. For each term in the above summation, the expectation can be computed as

$$\begin{aligned} & \mathbb{E}\{(1-m_{t,p})(1-m_{t,q})m_{t,\overline{p-k}}m_{t,\overline{q-l}}\} \\ &= \begin{cases} \rho^2(1-\rho)^2, & p \neq q, k \neq l, \overline{p-k} \neq \overline{q-l}; \\ \rho(1-\rho)^2, & p \neq q, k \neq l, \overline{p-k} = \overline{q-l}; \\ \rho^2(1-\rho), & p = q, k \neq l; \\ \rho^2(1-\rho)^2, & p \neq q, k = l; \\ \rho(1-\rho), & p = q, k = l. \end{cases} \quad (62) \end{aligned}$$

Using (62), and counting the terms of each type in the summation, we obtain

$$\begin{aligned} & \mathbb{E}\left\{\frac{1}{N-1} \sum_{k=1}^{N-1} \left(a_k - \frac{1}{N-1} \sum_{l=1}^{N-1} a_l\right)^2\right\} \\ &= \frac{N-2}{N-1} (N(N-1)\rho^2(1-\rho)^2 + N\rho(1-\rho)) \\ &+ \frac{1}{(N-1)^2} [(N-1)(N-2)^2 N\rho^2(1-\rho)^2 + (N-1) \\ &\times (N-2)N\rho(1-\rho)^2 + (N-1)(N-2)N\rho^2(1-\rho)], \end{aligned}$$

which can be simplified into (32). \blacksquare

D. Proof of Lemma 3

Proof: Let us first write the expected partial RGI as

$$\begin{aligned} \text{EPRGI}_k(\mathcal{B}) &= \mathbb{E}\{|r_{k,k}|^2\} - \frac{2}{N-|\mathcal{B}|} \sum_{q \in \overline{\mathcal{B}}} \text{Re} \left[\mathbb{E}\{(r_{k,k})^* r_{q,q}\} \right] \\ &+ \frac{1}{(N-|\mathcal{B}|)^2} \sum_{l \in \overline{\mathcal{B}}} \sum_{p \in \overline{\mathcal{B}}} \mathbb{E}\{(r_{l,l})^* r_{p,p}\}. \quad (63) \end{aligned}$$

The term $\mathbb{E}\{|r_{k,k}|^2\}$ can be written as

$$\begin{aligned} \mathbb{E}\{|r_{k,k}|^2\} &= \mathbb{E}\left\{ \left\| (\mathbf{1} - \mathbf{m}_t) \odot \left[\tilde{\mathbf{J}}_k(\mathbf{m}_t \odot \mathbf{x}_i) \right] \right\|^2 \right\} \\ &= \mathbb{E}\left[\mathbf{1}^T \left[(\mathbf{1} - \mathbf{m}_t) \odot \tilde{\mathbf{J}}_k(\mathbf{m}_t \odot \mathbf{x}_i) \right]^2 \right] \\ &= [(\mathbf{1} - \mathbf{m}_t) \odot \tilde{\mathbf{J}}_k \mathbf{m}_t]^T \mathbf{S} [(\mathbf{1} - \mathbf{m}_t) \odot \tilde{\mathbf{J}}_k \mathbf{m}_t] \\ &= |a_k|^2 + (\mu_4 - 1)a_k, \quad (64) \end{aligned}$$

while the cross terms $\mathbb{E}\{(r_{l,l})^* r_{p,p}\}$ can be computed as

$$\begin{aligned} \mathbb{E}\{(r_{l,l})^* r_{p,p}\} &= [(\mathbf{1} - \mathbf{m}_t) \odot \tilde{\mathbf{J}}_l \mathbf{m}_t]^T \tilde{\mathbf{J}}_l \mathbf{S} \tilde{\mathbf{J}}_p^T \\ &\cdot [(\mathbf{1} - \mathbf{m}_t) \odot \tilde{\mathbf{J}}_p \mathbf{m}_t] \\ &= a_l a_p + (\mu_4 - 1)(a_l - b_{lp}). \quad (65) \end{aligned}$$

Substituting (64) and (65) into (63) yields (49). \blacksquare

APPENDIX II SIDELOBE ANALYSIS

A. Proof of Proposition 5

Proof: From (7), the sidelobes can be rewritten as

$$\begin{aligned} r_{k,l} &= [\mathbf{0}_{N+l}; \mathbf{m}_t \odot \mathbf{x}_i; \mathbf{0}_{N-l}]^H (\mathbf{I}_3 \otimes \mathbf{M}_t) \\ &\cdot [[\mathbf{m}_t \odot \mathbf{x}_{i+1}]_{N-k+1:N}; \mathbf{m}_t \odot \mathbf{x}_{i-1}; \mathbf{m}_t \odot \mathbf{x}_i; \\ &\quad [\mathbf{m}_t \odot \mathbf{x}_{i+1}]_{1:N-k}] \\ &= (\mathbf{m}_t \odot \mathbf{x}_i)^H \tilde{\mathbf{J}}_l^H (\mathbf{I} - \mathbf{M}_t) \tilde{\mathbf{J}}_k (\mathbf{m}_t \odot \tilde{\mathbf{x}}_{i,k,l}), \quad (66) \end{aligned}$$

where $\tilde{\mathbf{x}}_{i,k,l}$ is given by

$$\tilde{\mathbf{x}}_{i,k,l} = \begin{cases} \tilde{\mathbf{J}}_k^H [[\mathbf{x}_i]_{N-k+1:N-k+l}; \\ \quad [\mathbf{x}_{i-1}]_{N-k+l+1:N}; [\mathbf{x}_i]_{1:N-k}], & k > l; \\ \tilde{\mathbf{J}}_k^H [[\mathbf{x}_i]_{N-k+1:N}; \\ \quad [\mathbf{x}_{i-1}]_{1:l-k}; [\mathbf{x}_i]_{l-k+1:N-k}], & k < l; \\ \mathbf{x}_i, & k = l. \end{cases}$$

For data payload signals, we have

$$r_{k,l} = \sum_{n=1}^N [\mathbf{m}_t \odot \mathbf{x}_i^*]_{n-l} [\mathbf{m}_t \odot \tilde{\mathbf{x}}_{i,k,l}]_{n-k} (1 - m_{t,n}).$$

Thus the expected sidelobe level can be computed as

$$\begin{aligned} \mathbb{E}\{|r_{k,l}|^2\} &= \sum_{m=1}^N \sum_{n=1}^N m_{t,\overline{m-l}} m_{t,\overline{n-l}} m_{t,\overline{m-k}} m_{t,\overline{n-k}} \\ &\times \mathbb{E}\{[\mathbf{x}_i^*]_{m-l} [\mathbf{x}_i]_{n-l} [\tilde{\mathbf{x}}_{i,k,l}]_{m-k} [\tilde{\mathbf{x}}_{i,k,l}^*]_{n-k}\} \\ &\times (1 - m_{t,m})(1 - m_{t,n}). \end{aligned}$$

Note that the expectation $\mathbb{E}\{a^*bcd^*\}$, where $a = [\mathbf{x}_i]_{m-l}$, $b = [\mathbf{x}_i]_{n-l}$, $c = [\tilde{\mathbf{x}}_{i,k,l}]_{m-k}$ and $d = [\tilde{\mathbf{x}}_{i,k,l}]_{n-k}$, satisfies

$$\mathbb{E}\{a^*bcd^*\} = \begin{cases} \mu_4, & a = b = c = d; \\ 1, & a = b \neq c = d; \\ 1, & a = c \neq b = d; \\ 0, & a = d \neq b = c; \\ 0, & \text{otherwise,} \end{cases} \quad (67)$$

where the fourth line follows from the rotational symmetry assumption (Assumption 2). Also note that when $k \neq l$ (i.e., sidelobe), the cases corresponding to the first and the third lines never happen, since $[\mathbf{x}_i]_{m-l} = [\tilde{\mathbf{x}}_{i,k,l}]_{m-k}$ does not hold for any m . Therefore, we may focus on the case where the second line of (67) holds, namely when $m = n$, which leads to the following simplified expression for the expected sidelobe level

$$\begin{aligned} \mathbb{E}\{|r_{k,l}|^2\} &= \sum_{n=1}^N m_{t,\overline{n-l}} m_{t,\overline{n-k}} (1 - m_{t,n}) \\ &= [\mathbf{R}]_{k,l}, \quad \forall k \neq l, \quad (68) \end{aligned}$$

which completes the proof. \blacksquare

B. Proof of Proposition 6

Proof: We first note that for all $k = 0$ or $l = 0$, $\mathbb{E}\{|r_{k,l}|^2\} = 0$. This allows us to express the summation in a more compact form

$$\sum_{k=1}^{N-1} \sum_{l>0, l \neq k} \mathbb{E}\{|r_{k,l}|^2\} = \mathbf{1}^T \mathbf{R} \mathbf{1} - \text{Tr}\{\mathbf{R}\}.$$

For the first term, we have

$$\begin{aligned} \mathbf{1}^T \mathbf{R} \mathbf{1} &= N \mathbf{1}^T \mathbf{F}^H \text{diag}(\mathbf{F}^* \mathbf{m}_t^*) \mathbf{F} (\mathbf{I} - \mathbf{M}_t) \\ &\cdot \mathbf{F}^H \text{diag}(\mathbf{F} \mathbf{m}_t) \mathbf{F} \mathbf{1} \\ &= (\mathbf{1}^T \mathbf{m}_t)^2 \mathbf{1}^T (\mathbf{I} - \mathbf{M}_t) \mathbf{1} \\ &= \rho^2 (1 - \rho) N^3. \quad (69) \end{aligned}$$

The second term satisfies

$$\begin{aligned} \text{Tr}\{\mathbf{R}\} &= N \text{Tr}\{\mathbf{F}^H \text{diag}(\mathbf{F}^* \mathbf{m}_t^*) \mathbf{F} (\mathbf{I} - \mathbf{M}_t) \\ &\quad \mathbf{F}^H \text{diag}(\mathbf{F} \mathbf{m}_t) \mathbf{F}\} \\ &= N \text{Tr}\{\mathbf{F}^H \text{diag}(|\mathbf{F} \mathbf{m}_t|^2) \mathbf{F} (\mathbf{I} - \mathbf{M}_t)\} \\ &= \rho (1 - \rho) N^2. \quad (70) \end{aligned}$$

Combining (69) with (70) yields (37). ■

C. Proof of Proposition 7

Proof: It is known in the finite projective geometry literature [33] that $\mathbb{P}\mathbb{G}(n, q)$ has $\sum_{i=0}^n q^i = (q^{n+1} - 1)(q - 1)^{-1} = N$ points as well as N hyperplanes. For these points and hyperplanes, one may construct an $N \times N$ matrix \mathbf{A} , referred to as the incidence matrix, characterised by

$$[\mathbf{A}]_{i,j} = \begin{cases} 1, & \text{The } i\text{-th hyperplane contains the } j\text{-th point;} \\ 0, & \text{otherwise,} \end{cases}$$

given a specific numbering for the points and hyperplanes. Singer [33] proved that for all $\mathbb{P}\mathbb{G}(n, q)$, there exist at least one numbering such that the corresponding incidence matrix \mathbf{A} takes a cyclic form, i.e., in the form of (41). Now we may express the range response as follows

$$\begin{aligned} [\mathbf{R}]_{k,l} &= [\mathbf{A}(\mathbf{I} - \mathbf{M}_t)\mathbf{A}^T]_{k,l} \\ &= ([\mathbf{A}]_{k,:} \odot [\mathbf{A}]_{l,:})\mathbf{1} - ([\mathbf{A}]_{k,:} \odot [\mathbf{A}]_{l,:} \odot [\mathbf{A}]_{1,:})\mathbf{1}, \end{aligned}$$

where $[\mathbf{A}]_{k,:}$ is the incidence vector between the k -th hyperplane and all points. We note that $[\mathbf{A}]_{k,:} \odot [\mathbf{A}]_{l,:}$ is in fact the incidence vector between all points and the intersection of the k -th and the l -th hyperplanes. When $k = l$, the intersection is the k -th hyperplane itself, which contains $\sum_{i=0}^{n-1} q^i = (q^n - 1)(q - 1)^{-1}$ points since it is isomorphic to $\mathbb{P}\mathbb{G}(n - 1, q)$. This implies $([\mathbf{A}]_{k,:} \odot [\mathbf{A}]_{k,:})\mathbf{1} = (q^n - 1)(q - 1)^{-1}$, which in turn yields the expression of duty cycle in (42). When $k \neq l$, the intersection is thus isomorphic to $\mathbb{P}\mathbb{G}(n - 2, q)$, which contains $(q^{n-1} - 1)(q - 1)^{-1}$ points. Therefore we have

$$\begin{aligned} [\mathbf{R}]_{k,k} &= ([\mathbf{A}]_{k,:} \odot [\mathbf{A}]_{k,:})\mathbf{1} - ([\mathbf{A}]_{k,:} \odot [\mathbf{A}]_{1,:})\mathbf{1} \\ &= \frac{q^n - 1 - q^{n-1} + 1}{q - 1} \\ &= q^{n-1}, \end{aligned}$$

for all $k > 1$, which corresponds to the mainlobes of the range response. This also suggests that these transmission masks are range-glint-ideal.

Next, let us consider the sidelobes of the range response. Note that the expression $[\mathbf{A}]_{k,:} \odot [\mathbf{A}]_{l,:} \odot [\mathbf{A}]_{1,:}$ can be rewritten as

$$[\mathbf{A}]_{k,:} \odot [\mathbf{A}]_{l,:} \odot [\mathbf{A}]_{1,:} = ([\mathbf{A}]_{k,:} \odot [\mathbf{A}]_{1,:}) \odot ([\mathbf{A}]_{l,:} \odot [\mathbf{A}]_{1,:}),$$

which corresponds to the intersection of two $(n - 2)$ -dimensional finite projective spaces. The result can be isomorphic to either $\mathbb{P}\mathbb{G}(n - 2, q)$ or $\mathbb{P}\mathbb{G}(n - 3, q)$. In the latter case, the number of points contained in the intersection is minimal, given by

$$([\mathbf{A}]_{k,:} \odot [\mathbf{A}]_{l,:} \odot [\mathbf{A}]_{1,:})\mathbf{1} = \frac{q^{n-2} - 1}{q - 1}.$$

In light of this, the PESL can be written as

$$\begin{aligned} \max_{k>0, l>0, k \neq l} [\mathbf{R}]_{k,l} &= \frac{q^{n-1} - 1 - q^{n-2} + 1}{q - 1} \\ &= q^{n-2}. \end{aligned}$$

Now, substituting the duty cycle expression (42) into (40), we obtain

$$\begin{aligned} \max_{k>0, l>0, l \neq k} [\mathbf{R}]_{k,l} &\geq \left[\frac{\rho(1 - \rho)N^2(\rho N - 1)}{(N - 1)(N - 2)} \right] \\ &= \left[\frac{q^{2n-1} - q^n}{q^{n+1} - 2q + 1} \right]. \end{aligned} \quad (71)$$

Observe that

$$\begin{aligned} \frac{q^{2n-1} - q^n}{q^{n+1} - 2q + 1} &\leq \left[\frac{q^{2n-1} - q^n}{q^{n+1} - 2q + 1} \right] \\ &\leq \frac{q^{2n-1} + q^{n+1} - q^n - 2q + 1}{q^{n+1} - 2q + 1}, \end{aligned} \quad (72)$$

but

$$q^{2n-1} - q^n < q^{n-2}(q^{n+1} - 2q + 1) < q^{2n-1} + q^{n+1} - q^n - 2q + 1$$

also holds for all $n \geq 2$ and $q \geq 2$. This implies that

$$q^{n-2} = \left[\frac{q^{2n-1} - q^n}{q^{n+1} - 2q + 1} \right] \quad (73)$$

holds for all $n \geq 2$ and $q \geq 2$, which in turn implies that Singer CDSs achieve the lower bound of PESL given by Corollary 1. Therefore, we may conclude that these transmission masks are simultaneously range-glint-ideal and PESL-ideal, completing the proof. ■

APPENDIX III PROPERTIES OF SLOW-TIME MASM

A. Proof of Proposition 8

Proof: Let us first note that for all $k = 0, \dots, N - 1$, it follows that

$$\begin{aligned} a_{kT} &= \sum_{n=1}^N (1 - m_{t,n}) m_{t, \overline{n-kT}} \\ &= \sum_{p=0}^{L-1} \sum_{q=0}^{T-1} (1 - m_{t, pT+q+1}) m_{t, \overline{(p-k)T+q+1}} \\ &= T \sum_{p=1}^L (1 - \tilde{m}_{t,p}) \tilde{m}_{t, \overline{p-k}} \\ &= T \tilde{a}_k. \end{aligned} \quad (74)$$

Next, consider the difference $a_{kT+l+1} - a_{kT+l}$ for $1 < l < T$, which can be written as

$$\begin{aligned} a_{kT+l+1} - a_{kT+l} &= \sum_{p=0}^{L-1} \sum_{q=0}^{T-1} (m_{t, \overline{(p-k)T-(l-q)}} - m_{t, \overline{(p-k)T-(l-q-1)}}) \\ &\quad \times (1 - m_{t, pT+q+1}) \\ &= T \sum_{p=1}^L (\tilde{m}_{t, \overline{p-k-c_0}} - \tilde{m}_{t, \overline{p-k-c_1}}) (1 - \tilde{m}_{t,p}), \end{aligned} \quad (75)$$

where $c_0 = \lfloor (l - q)/T \rfloor$, and $c_1 = \lfloor (l - q - 1)/T \rfloor$. Observe that $c_0 = c_1$ holds except for $q = l$, for which $c_0 = 1$, $c_1 = 0$. This implies that

$$\begin{aligned} a_{kT+l+1} - a_{kT+l} &= \sum_{p=1}^L (\tilde{m}_{t, \overline{p-(k+1)}} - \tilde{m}_{t, \overline{p-k}}) (1 - \tilde{m}_{t,p}) \\ &= d_k. \end{aligned} \quad (76)$$

Combining (74) with (76), we obtain (51). ■

REFERENCES

- [1] ITU-R WP5D, "Draft New Recommendation ITU-R M. [IMT. Framework for 2030 and Beyond]," 2023.
- [2] M. Chafii, L. Bariah, S. Muhaidat, and M. Debbah, "Twelve scientific challenges for 6G: Rethinking the foundations of communications theory," *IEEE Commun. Surv. Tuts.*, vol. 25, no. 2, pp. 868–904, 2nd quart. 2023.
- [3] W. Saad, M. Bennis, and M. Chen, "A vision of 6G wireless systems: Applications, trends, technologies, and open research problems," *IEEE Netw.*, vol. 34, no. 3, pp. 134–142, 2019.
- [4] Y. Cui, F. Liu, X. Jing, and J. Mu, "Integrating sensing and communications for ubiquitous IoT: Applications, trends, and challenges," *IEEE Netw.*, vol. 35, no. 5, pp. 158–167, Sep. 2021.
- [5] X. Li, Y. Cui, J. A. Zhang, F. Liu, D. Zhang, and L. Hanzo, "Integrated human activity sensing and communications," *IEEE Commun. Mag.*, vol. 61, no. 5, pp. 90–96, May 2023.
- [6] C. Sturm and W. Wiesbeck, "Waveform design and signal processing aspects for fusion of wireless communications and radar sensing," *Proc. IEEE*, vol. 99, no. 7, pp. 1236–1259, Jul. 2011.
- [7] X. Chen, Z. Feng, Z. Wei, P. Zhang, and X. Yuan, "Code-division OFDM joint communication and sensing system for 6G machine-type communication," *IEEE Internet Things J.*, vol. 8, no. 15, pp. 12 093–12 105, 2021.
- [8] Y. Zeng, Y. Ma, and S. Sun, "Joint radar-communication with cyclic prefixed single carrier waveforms," *IEEE Trans. Veh. Technol.*, vol. 69, no. 4, pp. 4069–4079, 2020.
- [9] L. Gaudio, M. Kobayashi, G. Caire, and G. Colavolpe, "On the effectiveness of OTFS for joint radar parameter estimation and communication," *IEEE Trans. Wireless Commun.*, vol. 19, no. 9, pp. 5951–5965, 2020.
- [10] W. Yuan, L. Zhou, S. K. Dehkordi, S. Li, P. Fan, G. Caire, and H. V. Poor, "From OTFS to DD-ISAC: Integrating sensing and communications in the delay doppler domain," *IEEE Wireless Commun.*, vol. 31, no. 6, pp. 152–160, Dec. 2024.
- [11] F. Liu, Y. Zhang, Y. Xiong *et al.*, "OFDM achieves the lowest ranging sidelobe under random ISAC signaling," *arXiv preprint*, 2024. [Online]. Available: <https://arxiv.org/abs/2407.06691>
- [12] P. Kumari, J. Choi, N. González-Prelcic, and R. W. Heath, "IEEE 802.11ad-based radar: An approach to joint vehicular communication-radar system," *IEEE Trans. Veh. Technol.*, vol. 67, no. 4, pp. 3012–3027, Apr. 2018.
- [13] N. Zhao, Q. Chang, Y. Wang, X. Shen, and Y. Shen, "On the performance improvements of data-aided joint sensing and communication," in *Proc. 2022 Int. Symp. Wireless Commun. Syst. (ISWCS)*, Hangzhou, China, Oct. 2022, pp. 1–6.
- [14] Y. Xiong, F. Liu, Y. Cui, W. Yuan, T. X. Han, and G. Caire, "On the fundamental tradeoff of integrated sensing and communications under Gaussian channels," *IEEE Trans. Inf. Theory*, vol. 69, no. 9, pp. 5723–5751, Sep. 2023.
- [15] M. Ahmadipour, M. Kobayashi, M. Wigger, and G. Caire, "An information-theoretic approach to joint sensing and communication," *IEEE Trans. Inf. Theory*, vol. 70, no. 2, pp. 1124–1146, 2024.
- [16] A. Sabharwal, P. Schniter, D. Guo, D. W. Bliss, S. Rangarajan, and R. Wichman, "In-band full-duplex wireless: Challenges and opportunities," *IEEE J. Sel. Areas Commun.*, vol. 32, no. 9, pp. 1637–1652, 2014.
- [17] D. Xu, X. Yu, Y. Sun, D. W. K. Ng, and R. Schober, "Resource allocation for IRS-assisted full-duplex cognitive radio systems," *IEEE Trans. Commun.*, vol. 68, no. 12, pp. 7376–7394, Dec. 2020.
- [18] C. B. Barneto, S. D. Liyanarachchi, M. Heino, T. Riihonen, and M. Valkama, "Full duplex radio/radar technology: The enabler for advanced joint communication and sensing," *IEEE Wireless Commun.*, vol. 28, no. 1, pp. 82–88, Jan. 2021.
- [19] Z. Xiao and Y. Zeng, "Waveform design and performance analysis for full-duplex integrated sensing and communication," *IEEE J. Sel. Areas Commun.*, vol. 40, no. 6, pp. 1823–1837, Jun. 2022.
- [20] Z. Wang, X. Mu, and Y. Liu, "Bidirectional integrated sensing and communication: Full-duplex or half-duplex?" *IEEE Trans. Wireless Commun.*, vol. 23, no. 8, pp. 8184–8199, Aug. 2024.
- [21] M. C. Budge and J. S. R. German, *Basis Radar Analysis*, 2nd ed. Norwood, MA, USA: Artech House, 2020.
- [22] R. McAulay, "The effect of staggered PRF's on MTI signal detection," *IEEE Trans. Aerosp. Electron. Syst.*, vol. AES-9, no. 4, pp. 615–618, Apr. 1973.
- [23] F. R. Coutinho, A. L. Stakowian, and M. J. da Silva, "A fast and improved dual-PRT Doppler technique for industrial flow metering," *IEEE Sens. Lett.*, vol. 7, no. 9, pp. 1–4, Sep. 2023.
- [24] A. Aldharab and M. E. Davies, "Staggered coprime pulse repetition frequencies synthetic aperture radar (SCopSAR)," *IEEE Trans. Geo. Remote Sens.*, vol. 60, pp. 1–11, 2022.
- [25] M. Ispir and C. Candan, "On the design of staggered moving target indicator filters," *IET Radar, Sonar & Navigation*, vol. 10, no. 1, pp. 205–215, Jan. 2016.
- [26] L. Zhang, H. Li, and D. Guo, "Capacity of Gaussian channels with duty cycle and power constraints," *IEEE Trans. Inf. Theory*, vol. 60, no. 3, pp. 1615–1629, Mar. 2014.
- [27] D. R. Morrison, S. H. Jacobson, J. J. Sauppe, and E. C. Sewell, "Branch-and-bound algorithms: A survey of recent advances in searching, branching, and pruning," *Discrete Optimization*, vol. 19, pp. 79–102, 2016.
- [28] T. Helleseth and G. Gong, "New nonbinary sequences with ideal two-level autocorrelation," *IEEE Trans. Inf. Theory*, vol. 48, no. 11, pp. 2868–2872, Nov. 2002.
- [29] J. Jensen, H. Jensen, and T. Hoholdt, "The merit factor of binary sequences related to difference sets," *IEEE Trans. Inf. Theory*, vol. 37, no. 3, pp. 617–626, Mar. 1991.
- [30] D. M. Gordon, "La Jolla difference sets repository (1.1)." [Online]. Available: <https://doi.org/10.5281/zenodo.13886556>
- [31] R. Scholtz and L. Welch, "GMW sequences (corresp.)," *IEEE Trans. Inf. Theory*, vol. 30, no. 3, pp. 548–553, Mar. 1984.
- [32] K. H. Leung and S. L. Ma, "Partial difference sets with Paley parameters," *Bulletin of the London Mathematical Society*, vol. 27, no. 6, pp. 553–564, Nov. 1995.
- [33] J. Singer, "A theorem in finite projective geometry and some applications to number theory," *Trans. American Math. Soc.*, vol. 43, no. 3, pp. 377–385, 1938.
- [34] J. F. Dillon and H. Dobbertin, "New cyclic difference sets with Singer parameters," *Finite Fields and Their Applications*, vol. 10, no. 3, pp. 342–389, 2004.
- [35] M. I. Skolnik, *Radar Handbook*, 2nd ed. New York, USA: McGraw-Hill, New York, 1990.